Quantum Electronics **34** (10) 881 – 900 (2004)

REVIEW

PACS numbers: 42.55.Wd; 42.60.By; 42.60.Jf; 42.60.Lh
DOI: 10.1070/QE2004v034n10ABEH002739

Moderate-power cw fibre lasers

A.S. Kurkov, E.M. Dianov

Contents

***Abstract*. A review of the development and investigation of moderate-power ($10^{-1} - 10^2$ W) cw fibre lasers is presented. The properties of optical fibres doped with rare-earth ions and methods for fabricating double-clad fibres are considered. The methods for fabrication of fibre Bragg gratings used as selective reflectors are discussed and the grating properties are analysed. The main pump schemes for double-clad fibre lasers are described. The properties of fibre lasers doped with neodymium, ytterbium, erbium, thulium, and holmium ions are also considered. The principles of fabrication of Raman converters of laser radiation based on optical fibres of different compositions are discussed and the main results of their studies are presented. It is concluded that fibre lasers described in the review can produce moderate-power radiation at any wavelength in the spectral range from 0.9 to 2 μm.**

Keywords: *fibre laser, active optical fibres, stimulated Raman scattering.*

A.S. Kurkov, E.M. Dianov Fiber Optics Research Center, A.M. Prokhorov General Physics Institute, Russian Academy of Sciences, ul. Vavilova 38, 119991 Moscow, Russia

Received 15 April 2004
Kvantovaya Elektronika **34** (10) 881 – 900 (2004)
Translated by M.N. Sapozhnikov

1. Introduction

Fibre lasers are one of the most spectacular achievements of modern quantum electronics. This line of investigation has appeared in the intermediate field between laser physics and fibre optics. Fibre lasers offer a number of advantages over conventional lasers and can be used along with conventional lasers and even replace them in some cases. Note that the main task of fibre optics at the beginning was the development of optical fibres as a passive medium for communication. However, as in any developing field of science, new possibilities of fibre optics were found during

solving the initial task, which resulted in the expansion of the scope of objects and phenomena being studied and, in turn, expanded the field of applications of optical fibres and devices based on them.

One of the fields of fibre optics is the development and investigation of fibre lasers. The active medium of these lasers are optical fibres doped with various impurities, first of all rare-earth elements. Note that the first fibre laser was fabricated by Snitzer in 1961, who demonstrated lasing in a glass doped with Nd^{3+} ions [1]. The active element of the laser was a glass filament covered with a cladding made of glass with a lower refractive index. The development of technologies for production of optical fibres and semiconductor pump sources inspired interest in fibre lasers at a qualitatively new level. This field of research began to develop rapidly in the late 1980s, when its was shown that optical fibres doped with Er^{3+} ions could find applications in fibre amplifiers in the wavelength range between 1.53 and 1.56 μm [2], i.e., in the spectral region of minimal optical losses of silica fibres. Studies of fibre amplifiers stimulated the development of high-power semiconductor pump sources. The discovery of the photorefractive effect in fibres [3] and the development of the fibre-Bragg-grating writing process [4] made it possible to produce Bragg mirrors forming a resonator directly in optical fibres and to obtain a variety of the all-fibre laser configurations. All this resulted in a rapid development of fibre lasers.

Note that the concept of 'fibre lasers' encompasses numerous laser configurations, which are characterised by substantially different output powers and different spectral and temporal properties of output radiation. In this paper, we consider cw fibre lasers, which attract great recent attention due to a variety of the applications, both realised and promising.

The classification of fibre lasers according to their output power is rather conditional, reflecting at the same time the features of the laser design. Thus, low-power lasers are pumped into the fibre core. This restricts the parameters of a pump semiconductor laser, whose emitting region should have a dimension of the order of 5–10 μm. In this case, the pump power does not exceed a few hundred milliwatts, so that the typical output power of such lasers is in the range from 10^{-1} to 10^{2} mW. Among these devices are fibre lasers emitting a single longitudinal mode with the linewidth of ~20 kHz [5, 6]. Low-power fibre lasers are used as radiation sources in optical communication systems and fibre sensors, as well in spectroscopy.

The development of high-power semiconductor lasers with a broad emitting region stimulated the elaboration of moderate-power cw fibre lasers emitting from a few hundred milliwatts to a few ten watts. These lasers use double-clad optical fibres with a core doped with active ions. As mirrors in moderate-power lasers, fibre Bragg gratings (FBGs) are commonly used. In this case, there are no bulk elements in the laser and, as a rule, no nonlinear-optical effects appear in the resonator. These lasers do not require any special provisions for eliminating the radiation breakdown of the fibre material. The conventional maximum output power of such lasers is a few ten watts in a single transverse mode.

Note that the output power exceeding 1 W is sufficient for exciting stimulated Raman scattering (SRS) in optical fibres to convert efficiently radiation of the fibre laser to radiation at a different wavelength [7]. Moderate-power fibre lasers and Raman converters are used for pumping erbium and Raman amplifiers operating in various spectral regions. In addition, they can be used in medicine, material machining, optical ranging, guidance systems, and wireless optical communication. Note that such a broad scope of applications is possible to a great extent due to the use of various rare-earth dopants in combination with Raman converters, which permit the fabrication of fibre lasers emitting virtually at any wavelength in the spectral range 0.9–2 μm.

For the last few years, high-power fibre lasers have been extensively developed. The output power of such lasers exceeds 100 W in a single transverse mode [8–11] and 1 kW in the multimode regime [12, 13]. A specific feature of these lasers is the use of bulk mirrors, which assumes the necessity of laser alignment. Obviously, the advantages of the all-fibre design, in which all the elements are connected by standard splicing of fibres, are lost in this case. In addition, active fibres, used in high-power single-mode lasers, have a rather large diameter of the fibre core (up to 30 μm), which complicates their joining with commercial optical fibres. High-power multimode lasers consist of single-mode fibre lasers assembled in a bunch. High-power fibre lasers are mainly used for material machining and in medicine.

Therefore, fibre lasers, which have been initially developed for the use in fibreoptic communications, begin to acquire now their own importance. This allows one to consider the development and investigation of such lasers as an independent field in quantum electronics and fibre optics. The fact that fibre lasers have already found a variety of applications, which can be further expanded, makes studies in this field urgent.

In this paper, we present a review of the main results in the development and investigation of moderate-power cw fibre lasers. Their design, which offer all advantages of the all-fibre configuration, is now generally accepted. It is these lasers that find now the widest application. We consider the properties of active media for moderate-power cw fibre lasers, the fabrication of the lasers and their pumping, as well as Raman lasers based on optical fibres with fibre cores of different chemical compositions.

2. Elements of a fibre laser

Figure 1 shows a simplest configuration of an end-pumped fibre laser consisting of a pump semiconductor laser with a pig tail, an optical fibre doped with active ions, and FBGs (other pump schemes will be considered below). The reflectivity of the input FBG is typically close to unity at the laser wavelength, while the required reflectivity of the

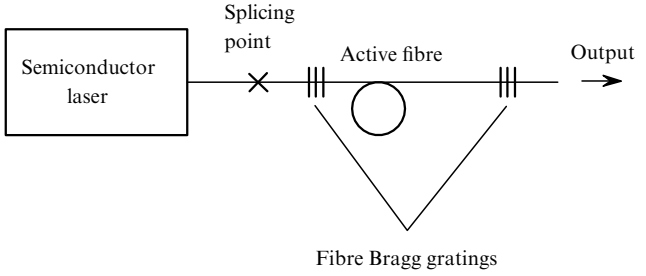

Figure 1. Simplest configuration of a fibre laser.

output grating is determined by the gain and optical losses in the active fibre. FBGs can be written both directly in the active fibre and in photosensitive fibres spliced to the active fibre. Consider individual elements of the fibre laser and their properties.

2.1 Active dopants in optical fibres

As in the case of solid-state lasers, lanthanide and rare-earth ions are most often used as active dopants in optical fibres. The specific optical properties of these ions are determined by the fact that they have occupied outer shells, whereas the inner f shell is not completely filled. The presence of the unfilled inner shell leads to a distinct discrete structure of electronic transitions, which determines the use of rare-earth ions as active impurities.

The applicability of an active ion for doping silica fibres is determined by the following factors: first, it should have a radiative transition in the near-IR region, where a silica glass is transparent. Second, the phonon energy in a silica glass is 400 – 1100 cm^{-1}, so that the presence of energy levels with a narrow energy gap in the optical transition leads to nonradiative relaxation, which prevents the appearance of luminescence. For this reason, the ions presented in Table 1 are most often used as active dopants in optical fibres. Table 1 also gives the luminescence regions of these ions. Note that in optical fibres based on glasses of different compositions, for example fluoride and chalcogenide glasses, lasing was obtained using other active ions, for example, praseodymium. The energy level diagrams of ions presented in Table 1 are shown in Fig. 2.

Table 1. Rare-earth elements used for fabrication of active optical fibres and their luminescence regions.

Active ion	Luminescence region/μm
	0.92 – 0.94
Nd^{3+}	1.05 – 1.1
	1.34
Ho^{3+}	1.9 – 2.1
Er^{3+}	1.53 – 1.6
Tm^{3+}	1.7 – 1.9
Yb^{3+}	0.98 – 1.16

Neodymium (Nd^{3+}). Neodymium ions in a silica glass have a number of strong absorption bands in the visible and near-IR regions; however, selective excitation to the $^4F_{5/2}$ level is most often performed using a 0.8-μm semiconductor laser. Three main luminescence bands are located at 0.92, 1.06, and 1.34 μm. The most intense is the 1.06-μm band corresponding to the $^4F_{3/2} \rightarrow {}^4I_{11/2}$ transition. (The excited-state lifetime is ~ 0.5 ms.) The laser operates at this wavelength according the four-level scheme. For this reason, neodymium was the first active impurity used in a silica glass fibre laser [14].

Generation at the $^4F_{3/2} \rightarrow {}^4I_{9/2}$ transition ($\lambda \sim 0.92$ μm) in fibre lasers is complicated due to competition with luminescence at 1.06 μm, while generation at 1.34 μm [the ($^4F_{3/2} \rightarrow {}^4I_{13/2}$) transition] is prevented due to excited-state absorption. Nevertheless, the efficient fibre laser emitting at 0.92 μm was fabricated by suppressing luminescence at 1.06 μm [15].

Holmium (Ho^{3+}). As shown in Ref. [16], Ho^{3+} has the $^5I_7 \rightarrow {}^5I_8$ laser transition corresponding to emission at 2 μm.

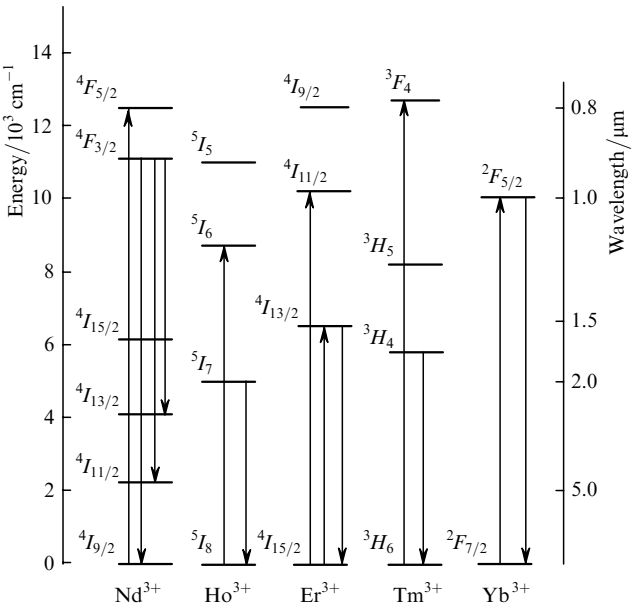

Figure 2. Energy level diagram of rare-earth ions.

The excited-state lifetime is about 0.5 ms. The holmium laser should operate according to the three-level scheme because ground-state absorption occurs at the same wavelength. Therefore, to obtain the population inversion in such lasers, pumping should be performed into an intense absorption band. For this reason, solid-state holmium lasers pumped by flashlamps into absorption bands in the visible region found the most common use. The 0.9-μm absorption band corresponding to the $^5I_8 \rightarrow {}^5I_5$ transition was not used for pumping by a semiconductor laser because of the low intensity of the band. At the same time, the presence of the intense absorption band at 1.15 μm corresponding to the $^5I_8 \rightarrow {}^5I_6$ transition suggests the possibility of improving the characteristic of the holmium-doped fibre laser by pumping into this band. As will be shown below, this was achieved upon pumping by an ytterbium-doped fibre laser [17].

Erbium (Er^{3+}). Erbium ions in a silica glass exhibit the $^4I_{13/2} \rightarrow {}^4I_{15/2}$ laser transition corresponding to emission at 1.53 – 1.6 μm, the metastable-level lifetime being 10 – 12 ms. This spectral range coincides with the range of minimum optical losses in silica fibres and, hence, with the spectral range used in modern fibreoptic communication links. In combination with pump semiconductor lasers emitting at 0.98 and 1.45 – 1.48 μm, this resulted in wide applications of erbium-doped fibres and devices based on them. Note that the quantum efficiency of pumping these fibres approaches 100 %, while a long lifetime of the metastable level (~ 10 ms) provides high gains. The properties of erbium-doped fibres are considered in several monographs, in particular in Ref. [18, 19].

Thulium (Tm^{3+}). Lasing of a silica glass doped with thulium ions was demonstrated in Ref. [20]. Lasing was observed at the $^3H_4 \rightarrow {}^3H_6$ transition by pumping into the absorption bands corresponding to the transition to the $^3F_4$ level (~ 790 nm) or to the $^3H_5$ level (1060 – 1250 nm). The spectral range of lasing was 1850 – 2100 nm, and the metastable-level lifetime was ~ 0.2 ms. Lasing in a Tm^{3+}-doped fibre was first demonstrated in Ref. [21].

Ytterbium (Yb^{3+}). The energy level diagram of Yb^{3+} ions is very simple. Except the $^2F_{7/2}$ ground-state level, the ytterbium ion has only one level $^2F_{5/2}$. Therefore, the absorption spectrum of Yb^{3+}-doped fibres consists of only one absorption band, which has a complicated shape due to the Stark splitting. This band exhibits two maxima at 915 and 976 nm, and pumping is performed by semiconductor lasers emitting in these spectral ranges. The luminescence spectrum corresponding to the $^2F_{5/2} \rightarrow {}^2F_{7/2}$ transition has maxima in the regions 978–982 nm and 1030–1040 nm, extending up to 1.15–1.2 μm. The metastable-level lifetime in an aluminosilicate glass is ~ 0.8 ms. This makes it possible to fabricate various fibre lasers with different spectral and energy parameters emitting in the range from 0.98 to 1.2 μm [22, 23].

2.2 Photoinduced refractive-index gratings

Photoinduced refractive-index FBGs are used in fibre lasers as selective mirrors forming the laser resonator. The production of FBGs became possible after the discovery of the photosensitivity of optical fibres, i.e., a stable variation in the refractive index in the core of an optical fibre induced by UV radiation at certain wavelengths. At present many studies devoted to this problem were reported and monograph [24] published. In the general case, a photoinduced FBG is a piece of an optical fibre with the modulated refractive index of the fibre core with the amplitude at a level of $10^{-5} - 10^{-3}$ and modulation period of the order of the wavelength of light.

The main parameters of the FBG are the index-modulation period Λ, the induced variation δn in the refractive index, the number N of lines or the length L of the FBG. Two modes interact on the grating with the period Λ if their propagation constants β_1 and β_2 satisfy the phase-matching condition

$$\beta_2 - \beta_1 = \frac{2\pi m}{\Lambda}, \tag{1}$$

where m is an integer characterising the grating order in which the intermode interaction occurs. The coupling of the fundamental mode with the counterpropagating mode appears at a certain wavelength λ_{Br} determined by the relation

$$2n_{eff}\Lambda = \lambda_{Br}, \tag{2}$$

where n_{eff} is the effective refractive index for the fundamental mode of the fibre. As a result, reflection appears at the wavelength λ_{Br}. The parameters of gratings (spectral width and reflectivity) can be varied in a broad range depending on the writing conditions and photosensitivity of the fibre. The reflectivity R of a uniform FBG of length L is determined by the expression [25]

$$R = th^2(kL), \tag{3}$$

where $k = \pi\eta\delta n/\lambda_{Br}$ is the coupling coefficient; η is the fraction of radiation power propagating in the region with modulated refractive index. The FWHM of the resonance is described by the expression [26]

$$\Delta\lambda = \lambda\alpha\left[\left(\frac{\delta n}{2n}\right)^2 + \left(\frac{1}{N}\right)^2\right]^{1/2}, \tag{4}$$

where α is the parameter that is approximately equal to unity for deep gratings ($R \sim 1$) and 0.5 for gratings with a small depth.

Because the FBG period is less than 1 μm for reflection in the near-IR region, the grating is produced by the interferometric method using UV radiation. Figure 3 shows the scheme for FBG writing using a Lloyd interferometer. Note that such a scheme requires a high spatial coherence of radiation and for this reason it uses, as a rule, the 244-nm second harmonic of an argon laser.

Another method for FBG writing is the phase-mask method [27]. This method is based on the interference of the +1st and −1st diffraction orders of radiation propagated though a silica phase mask with a relief designed to suppress the zero and other diffraction orders. The requirements to the coherence of a radiation source in this method are not very strict, which allows the use of KrF (248 nm) and ArF (193 nm) excimer lasers.

Figure 4 shows the typical transmission spectrum of a FBG with the parameters $L = 5$ mm, and $\delta n = 8 \times 10^{-4}$, $\Lambda = 0.4$ μm. The grating provides the reflectivity $R \sim 0.99$ at a wavelength of 1136 nm, the width of the reflection spectrum being ~ 0.4 nm. Such gratings, having a high

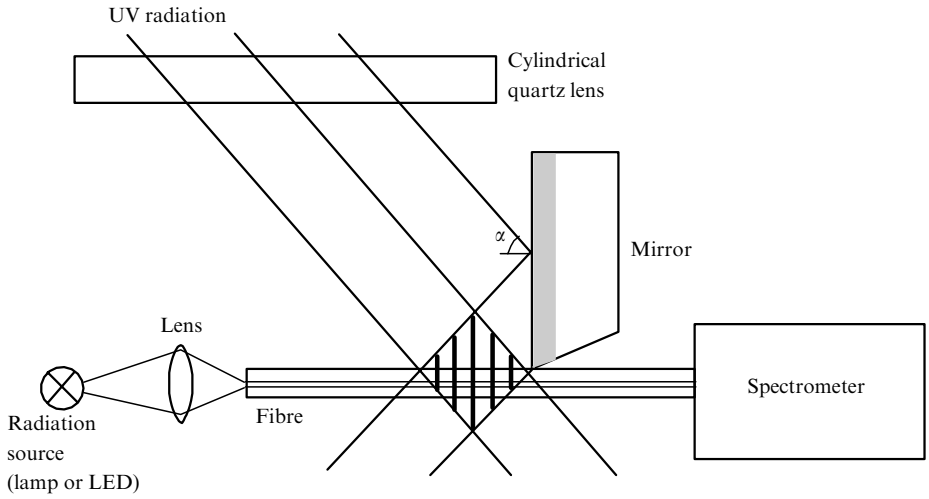

Figure 3. Scheme for FBG writing using a Lloyd interferometer.

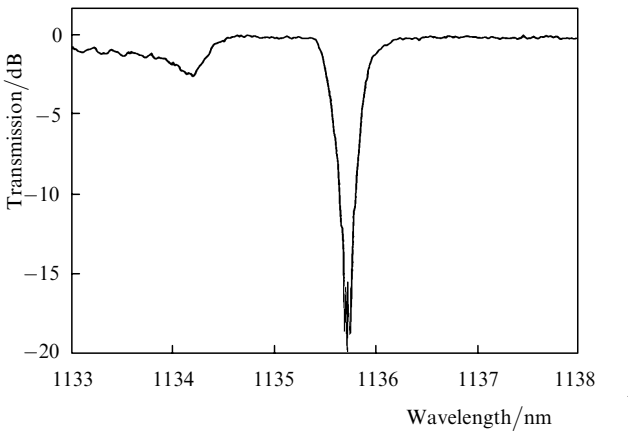

Figure 4. Typical transmission spectrum of a FBG with the parameters $L = 5$ mm and $\delta n = 8 \times 10^{-4}$.

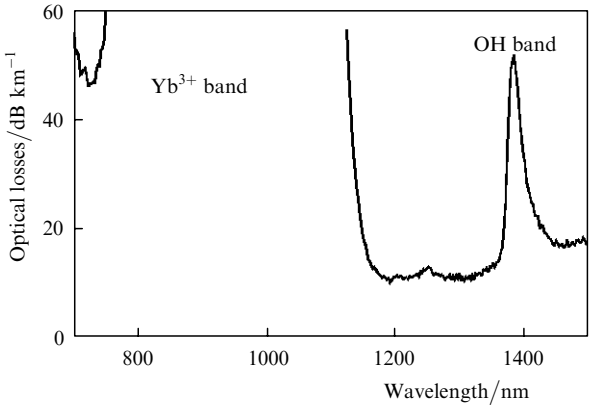

Figure 5. Spectrum of optical losses in the fibre core at the Yb^{3+}-ion concentration equal to 8×10^{19} cm^{-3}.

reflectivity and a large width of the reflection spectrum, are commonly used as input mirrors in fibre lasers.

2.3 Active optical fibres

Optical fibres doped with ions having optical transitions are called active fibres. The active ion can be doped both into the core of a fibre and into its reflecting cladding if a noticeable fraction of optical power propagates in the latter. Active fibres are produced using a number of technological processes: MCVD (modified chemical vapour deposition) [28, 29], OVD (outer vapour deposition) [30], VAD (vapour axial deposition) [31], PCVD (plasma chemical vapour deposition) and SPCVD [32, 33]. The active impurity is doped in these processes, as a rule, by the impregnation method, when a non-melted porous core material is impregnated with the solution of the active impurity salt, or by doping from volatile compounds.

Note that the maximum concentration of active ions in the silica glass network is low and is restricted by their solubility and cooperative effects. As a result, the length of a fibre laser can achieve a few ten meters. Therefore, active optical fibres should have sufficiently low non-resonance optical loses. The acceptable value of losses is 5–20 dB km^{-1}. In this case, their influence on the laser efficiency does not exceed a few percent. Figure 5 shows the spectrum of optical losses for an optical fibre doped with Yb^{3+} ions at a concentration of 8×10^{19} cm^{-3} [34]. The core of this fibre was co-doped with Al_2O_3, which allows one to increase the solubility limit for rare-earth ions in a silica glass and to decrease the probability of their clustering, resulting in cooperative up-conversion [35].

As mentioned above, high-power semiconductor sources for pumping fibre lasers require the use of double-clad optical fibres. As the active medium for high-power fibre lasers, optical fibres are used which consist of a single-mode core doped with active rare-earth ions and with impurities forming the refractive-index profile, as well as of an inner silica cladding and outer cladding with the refractive index lower than that of a silica glass. The model profile of the refractive index for such fibres is shown in Fig. 6a.

The inner cladding (together with the outer cladding) forms a multimode fibre in which pump radiation propagates. The typical diameter of the inner cladding is 0.1–

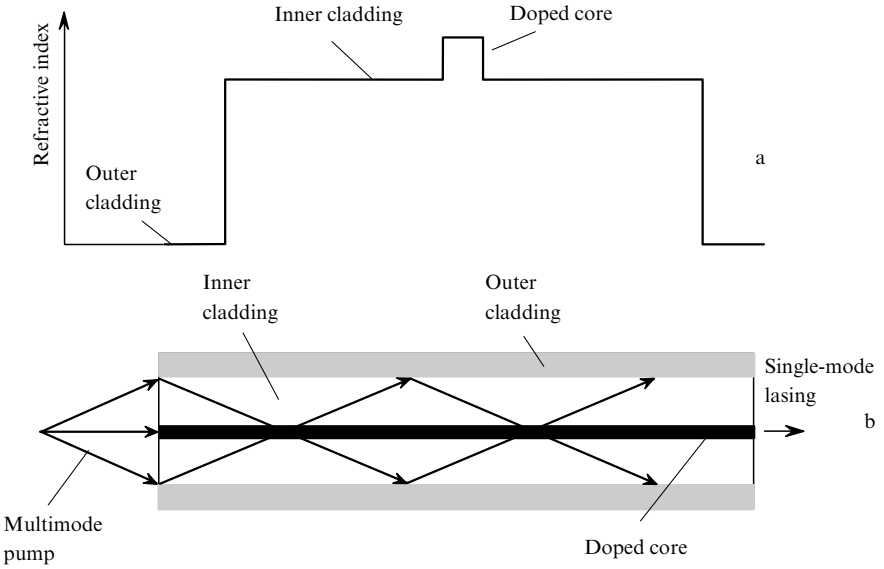

Figure 6. Model refractive-index profile (a) and the principle of conversion of multimode pump radiation to single-mode radiation of a fibre laser (b).

1 mm, which provides coupling of up to a few ten watts of pump radiation from semiconductor lasers. The pump radiation propagating in a multimode fibre is absorbed by active rare-earth ions, resulting in their luminescence, which can develop to lasing in the presence of feedback. The region of lasing is localised in a single-mode core, i.e., its typical transverse size is 5 – 10 μm [36, 37]. The principle of conversion of multimode pump radiation to single-mode radiation of a fibre laser is illustrated in Fig. 6b. Therefore, the cladding-pumped fibre laser can be considered as a device providing the enhancement of the brightness of a semiconductor laser by a few hundred times (of course, at a different wavelength).

The outer cladding of double-clad optical fibres is normally made of polymers with a low refractive index. In particular, silicon rubber is used, which provides the numerical aperture of a multimode fibre equal to NA = 0.38, and AF Teflon which increases NA to 0.6. As a rule, fibres with a polymer coating have an outer diameter of 100 – 300 μm.

A disadvantage of silicon coatings is the high level of optical losses for pump radiation, which can exceed 50 dB km^{-1}. The use of Teflon reduces optical losses in the cladding down to ~ 10 dB km^{-1}. In addition, Teflon has a high transmission in the UV region, which allows FBG writing without polymer removing. However, a Teflon coating is thin (10 – 20 μm) and thus cannot reliably protect the fibre from damage.

To provide the efficient coupling of modes in the inner cladding with the activated core, it is necessary to use fibres with the noncircular inner cladding [38], because otherwise a great part of radiation power will propagate in modes that do not intersect the fibre core. The efficiency of radiation absorption in optical fibres with inner claddings of different shapes was studied for several samples made of the same perform with the core doped with ytterbium [34]. The optical fibres had the following shape and parameters of the inner cladding: circular (diameter 125 μm), D-like with one polished face (125 × 100 μm), rectangular (150 × 75 μm), and square (125 × 125 μm). The absorption band of ytterbium was measured in straight fibres and fibres bent in the form of figure eight with the radius of curvature of 1 cm. The use of the latter configuration should provide the mixing of cladding modes and the increase in the intensity of the absorption band of Yb^{3+} if cladding modes are not coupled with the fibre core in a straight fibre. The results of the measurements presented in Table 2 show that the irregular fibre bending leads to a change in absorption only for a fibre with a circular inner cladding. Therefore, we can conclude that each noncircular inner cladding provides the efficiency of pump radiation absorption close to 100 %. The D-like shape seems simplest to fabricate because only one face of a preform should be ground off. However, the splicing of such a fibre with a fibre with a circular cladding used for FBG production leads to high losses because of its asymmetric shape. Therefore, the optimal shape of the cladding is a square, which provides both a high efficiency of radiation absorption and low optical losses in splicing with circular fibres. Note that other cladding shapes can be also used, in particular, a hexagonal shape.

In some cases, it is necessary to use active fibres with a small diameter (30 – 60 μm) of the inner cladding, which are pumped by higher-brightness semiconductor lasers. The use of fibres with a polymer coating is complicated due to their small diameter, which precludes the use of welders for splicing with other optical fibres. In this case, double-clad fibres made of silica glasses of different compositions [39] can be used. In such fibres, a silica supporting tube is used as the outer cladding, and the inner cladding is made of a silica glass containing GeO_2 at high concentration. A disadvantage of this structure is the restriction of the numerical aperture of the fibre because of the preform destruction due to a difference between the thermal expansion coefficients of materials of the inner and outer claddings. The probability of preform destruction increases at large sizes of the deposited cladding. For this reason, the numerical aperture for pump radiation in practice is 0.2 – 0.25, which considerably restricts the pump radiation coupled to the fibre.

Table 2. Effect of the inner-cladding geometry on the absorption of pump radiation in a Yb^{3+}-doped fibre.

Cladding geometry	Absorption at 978 nm/dB m^{-1}	
	straight fibre	'figure eight'
Circular	0.3 ± 0.05	0.6 ± 0.05
D-like	2.2 ± 0.05	2.2 ± 0.05
Rectangular	3.5 ± 0.05	3.5 ± 0.05
Square	3.3 ± 0.05	3.3 ± 0.05

Another variant is the use of an activated fibre with a microstructure cladding [40], whose cross section is shown in Fig. 7. The numerical aperture of such fibres is typically 0.5 and is limited by the leakage of higher-order modes through connectors supporting the inner cladding. A high value of the NA allows one to increase the pump density by several times compared to the previous design of fibres by using the same pump sources and the same diameter of the inner cladding.

2.4 Pump schemes for active optical fibres

Several methods were proposed for pumping active optical fibres. The simplest of them is end-pumping, when radiation from a semiconductor laser is coupled to the active fibre through its end (Fig. 1). An advantage of this method is that it can be used for all double-clad fibres described above. A disadvantage of the method is that only one pump source can be used (a laser diode or a diode array), so that

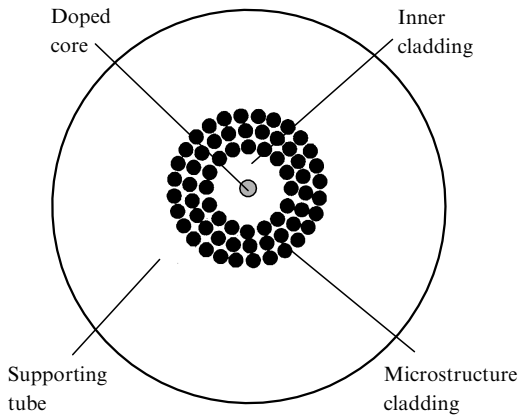

Figure 7. Scheme of a fibre with a microstructure cladding. Dark circles are air gaps.

optical power coupled to the fibre is restricted by the parameters of modern semiconductor lasers.

Two other pump schemes use the principle of distribution of coupled pump radiation over the active fibre length. Thus, it was proposed in Ref. [41] to couple pump radiation by using a set of V-grooves made on the side surface of the fibre. The principle of pump coupling is shown in Fig. 8. An obvious advantage of this method is the possibility of adding radiation sources along the active fibre length with decreasing power from a previous source. A disadvantage of the method is the necessity of fixing a semiconductor laser with respect to the active fibre and of protecting the region of radiation coupling from external perturbations.

A specific feature of another pump method is the use of a special double fibre consisting of two fibres with a common polymer jacket having the refractive index lower than that of a silica glass (GTW fibre). On of the fibres (active) has the core doped with ytterbium ions, while the second one (passive) is made of a high-purity silica glass [42] (Fig. 9). Pump radiation from a semiconductor laser is coupled into the passive fibre. The pump power coupled into the passive fibre is redistributed between the fibres in the region of their contact, the ratio of pump powers in both fibres being determined by the ratio of areas of their claddings. Absorption of a part of radiation in the active fibre core is compensated for by additional transfer of radiation from the passive fibre, which is required to maintain a constant ratio of pump powers in the active and passive fibres. Therefore, pump radiation is distributed over the entire length of the active fibre. In this scheme, two pump sources can be used for coupling radiation from the opposites ends of the passive fibre, and the passive fibre can be ruptured to add a new radiation source in the region of pump power depletion (Fig. 9). In addition, the number of passive fibres in the assembly can be increased, which makes it possible, in turn, to increase the number of pump sources.

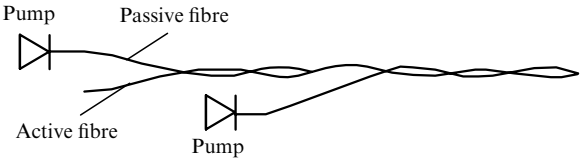

Figure 9. Pump scheme using a double fibre.

2.5 Specific features of optical fibres as amplifiers

Active optical fibres as amplifiers have a number of specific features compared to laser crystals and glasses. Thus, the guided propagation of pump and signal photons excludes, as a rule, radiative losses through the fibre surface. Radiative losses can appear only when the fibre parameters have been selected inappropriately or when the fibre has a small-radius bending. This is an obvious advantage of fibre lasers over traditional solid-state lasers. However, because the typical length of the active medium of fibre lasers is a few metres or ten metres, they efficiency should be analysed by taking into account the non-resonance optical losses both for pump and signal radiation.

The other features of fibre lasers are determined by the fact that radiation propagates not only in the core of a single-mode fibre but also in its reflecting cladding, and the fractions of the optical power in the core and cladding can be comparable. In addition, an active impurity can be doped not into the entire core but only into its part or into a part of the cladding. In principle, different regions of a fibre can be doped with different active impurities. In this case, the ions do not interact with each other in the accepted sense, but are only optically coupled.

Therefore, classical expressions for the gain in the case of optical fibres should be modified. Let us present the relations for the evolution of the signal and pump powers for the three-level amplification scheme according to which most fibre lasers operate:

$$\frac{dP_s}{dz} = \chi_s[N_1\sigma_e(\lambda_s) - N_0\sigma_a(\lambda_s)]P_s - \alpha_s P_s, \tag{5}$$

$$\frac{dP_p}{dz} = -\chi_p N_0 \sigma_a(\lambda_p) P_p - \alpha_p P_p, \tag{6}$$

where P_s and P_p, λ_s and λ_p are powers and wavelengths of the signal and pump, respectively; σ_a and σ_e are the absorption and luminescence cross sections; N_0 and N_1 are the populations of the ground and metastable levels; α_s and α_p are the coefficients of non-resonance losses for the signal and pump; χ_s and χ_p are the overlap integrals of the

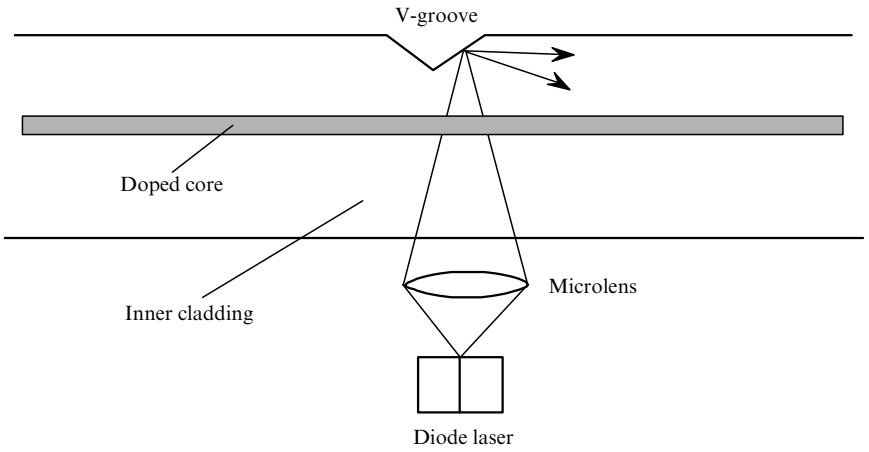

Figure 8. Scheme of pumping through a V-groove.

radiation fields of the signal and pump with the active region,

$$\chi_{s,p} = \frac{\int_{r_1}^{r_2} E_{s,p}(r) 2\pi r \mathrm{d}r}{\int_0^{\infty} E_{s,p}(r) 2\pi r \mathrm{d}r}, \quad (7)$$

where $E(r)$ is the radial distribution of the corresponding field; r_1 and r_2 are the boundaries of the fibre region doped with active ions.

Upon pumping into the fibre cladding, the value of χ_p can be estimated approximately as

$$\chi_p \simeq \frac{S_d}{S_{cl}}, \quad (8)$$

where S_d and S_{cl} are the cross sections of the doped region and cladding, in which pump radiation propagates. Note that relation (8) is only approximate because the overlap integral for the pump radiation depends in this case on the distribution of the pump radiation intensity, the excitation method, the cladding shape, etc. Nevertheless, it is clear that pumping into the fibre cladding is equivalent to a substantial decrease in the absorption cross section at the pump wavelength.

3. Fabrication of Raman lasers

Raman fibre converters can efficiently convert pump laser radiation to lower-frequency radiation (Stokes radiation) by using stimulated Raman scattering (SRS) of light in an optical fibre. The SRS of laser radiation in a glass fibre was observed in 1971 [43]. Glass fibres with low optical losses developed shortly before by Corning Glass were used in experiments.

In the case of cw pumping, the initial growth of the Stokes wave intensity is described by the expression

$$\frac{\mathrm{d}I_s}{\mathrm{d}z} = g_R I_p I_s, \quad (9)$$

where I_s is the Stokes wave intensity; I_p is the pump wave intensity; and g_R is the SRS gain.

A specific feature of optical fibres as a SRS medium is their relatively low gain. Thus, for fused silica, from which optical fibres are mainly produced, the gain is $\sim 10^{-13}$ m W^{-1} [43]. In addition, the number of dopants that can be used for changing the spectrum and SRS gain in optical fibres is limited by technological possibilities and the requirement of preserving low optical losses. On the other hand, silica fibres have a unique property such as a long interaction length, which reduces the SRS threshold. A silica glass itself as an amorphous material has a broad Raman spectrum with a maximum at 440 cm^{-1}. Doping with GeO_2 at concentrations used for fabricating optical fibres weakly changes the shape of the Raman spectrum. The Raman spectrum of a germanosilicate fibre is shown in Fig. 10 [curve (*1*)] [44].

By placing the active medium of the Raman converter in a resonator formed by narrow-band mirrors, we obtain a Raman laser. In the first works devoted to the development of Raman lasers, dielectric or metal mirrors deposited on a massive substrate were used, which made the laser rather bulky and required adjustment. The development of Raman lasers was considerably stimulated by the demonstration of their application for pumping Raman amplifiers [45, 46]. The use of fibre couplers and FBGs to obtain feedback in the resonator substantially simplified the Raman laser design, made this laser acceptable for applications and made it possible to develop multistage Raman converters.

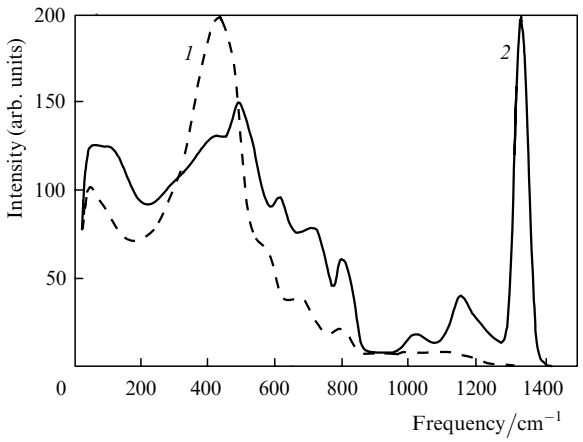

Figure 10. Raman spectra of germanosilicate (*1*) and phosphosilicate (*2*) fibres.

The Raman laser design was further simplified by using an active fibre with the core doped with phosphorous oxide [47]. The Stokes shift $\Delta\nu_{St}$ in this fibre is 1330 cm^{-1}, which is three times larger than that in a germanosilicate fibre (Fig. 10). The improvement of characteristics of phosphosilicate fibres [48] resulted in the development of Raman lasers competing in efficiency with Raman germanosilicate fibre lasers, but having a simpler design due to a smaller number of conversion stages and, hence, a smaller number of FBGs.

Figure 11 shows a simplified scheme of a multistage Raman laser. It is assumed in simulation that the fibre is single mode at the pump wavelength. In addition, it is assumed that other nonlinear effects, in particular stimulated Brillouin scattering, are not excited. The latter approximation is valid when pumping is performed by a fibre laser with a rather broad emission line. A Raman laser consists of an optical fibre and a set of FBGs with resonance wavelengths corresponding to Stokes shifts in the fibre. The gratings tuned to the intermediate wavelengths have the reflectivity close to 100%.

Raman lasers were theoretically studied in a number of papers [49 – 54]. The behaviour of a multistage converter can be described by the relations

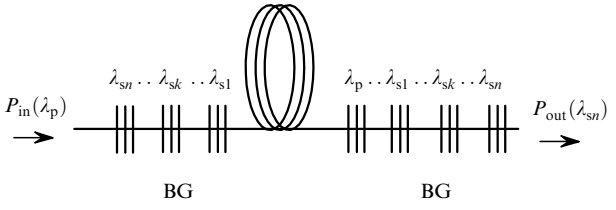

Figure 11. Simplified scheme of a multistage Raman converter (P_{in} is the input pump power; P_{out} is the output power at the nth conversion stage; $k = 1, \ldots, n$).

$$\frac{dP_p^{f,b}}{dz} = \mp\alpha_p P_p^{f,b} \mp \frac{\nu_p}{\nu_{s1}} \frac{g_R^1}{A_{eff}^1}(P_{s1}^f + P_{s1}^b)P_p^{f,b},$$

$$\frac{dP_{sk}^{f,b}}{dz} = \mp\alpha_{sk} P_{sk}^{f,b} \mp \frac{\nu_{sk}}{\nu_{sk+1}} \frac{g_R^{k+1}}{A_{eff}^{k+1}}(P_{sk+1}^f + P_{sk+1}^b)P_{sk}^{f,b} \pm \frac{g_R^k}{A_{eff}^k}(P_{sk-1}^f + P_{sk-1}^b)P_{sk}^{f,b}, \quad (10)$$

$$\frac{dP_{sn}^{f,b}}{dz} = \mp\alpha_{sn} P_{sn}^{f,b} \pm \frac{g_R^n}{A_{eff}^n}(P_{sn-1}^f + P_{sn-1}^b)P_{sn}^{f,b},$$

where P_p, and P_{sk} are the pump and signal powers at intermediate frequencies; P_{sn} is the signal power at the final wavelength; indices f and b describe the forward and backward waves; ν_p and ν_{sk} are the pump and signal frequencies; the ν_p/ν_{sk} ratio takes into account the difference in the energies of photons; α_p, and α_{sk} are the coefficients of linear losses at the pump and signal waves; and A_{eff} is the effective area occupied by the mode.

Note that it is difficult to measure the parameters g_R and A_{eff} with a sufficient accuracy. Because of this, the integral characteristic – the gain G of the optical fibre at a specified wavelength,

$$G = \frac{g_R}{A_{eff}} \quad (11)$$

which can be readily measured, can be used in calculations.

The numerical calculation based on the above relations is used to optimise the parameters of the converter by selecting the fibre length inside the converter and the reflectivity of a FBG with the resonance wavelength corresponding to the output signal for the specified power of the input signal and parameters of the optical fibre.

4. Characteristics of fibre lasers

In this section, we consider the characteristics of fibre lasers based on fibres doped with different rare-earth elements.

4.1 Nd^{3+}-doped fibre lasers

A Nd^{3+}-doped fibre laser emitting at 1.06 μm was the first laser in which pumping into cladding was used [55]. This was done because the first high-power semiconductor lasers had a low brightness, and to couple pump radiation it was necessary to use active fibres with the inner cladding diameter of a few hundred micrometres. As a result, the population inversion was low, and lasing could be achieved only in four-level systems, where signal reabsorption is absent.

During several years after the first publication, the output power of neodymium lasers [57] exceeded 30 W [56]. Figure 12 shows the typical characteristics (spectrum and power) of the Nd^{3+}-doped fibre laser having the 290 × 290-μm fibre cladding and the activated core of diameter 5 μm. The laser was pumped at 0.81 μm by a diode array.

In Ref. [58], a fibre laser emitting simultaneously at two wavelengths of 1060 and 1090 nm was demonstrated. The fibre core was doped with aluminium and germanium. The active ions were located in different surroundings and had different luminescence spectra. Upon 8.5-W pumping, the laser emitted more than 3 W at 1060 nm and more than 1 W at 1090 nm.

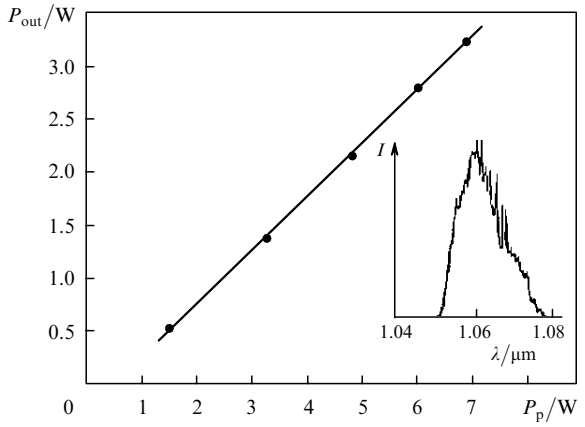

Figure 12. Dependence of the output power of a Nd^{3+}-doped fibre laser on the pump power. The inset shows the emission spectrum of the laser.

Of great interest is the development of a neodymium laser emitting at 0.92 μm. Such lasers can be used for pumping an ytterbium-doped fibre laser emitting at 0.98 μm. In turn, the ytterbium laser, having a rather high power, can be used for pumping erbium-doped fibre amplifiers. The neodymium laser also can be used for frequency doubling to obtain blue emission.

As mentioned above, it is difficult to produce lasing at the $^4F_{3/2} \rightarrow {}^4I_{9/2}$ transition in the Nd^{3+}-doped laser due to the competition with luminescence at 1.06 μm. Therefore, the main problem in this case is the suppression of luminescence in this region. In Ref. [15], a special optical fibre was used with the waveguide structure having high radiation losses in the spectral region >1 μm. This allowed the authors [15] to obtain lasing with the 0.5-W output power at 925 nm. The emission spectrum of this laser is shown in Fig. 13. One can see that the suppression of luminescence at 1060 nm was about 60 dB. Figure 14 shows the dependence of the output power on the pump power. The slope lasing efficiency was about 35 %.

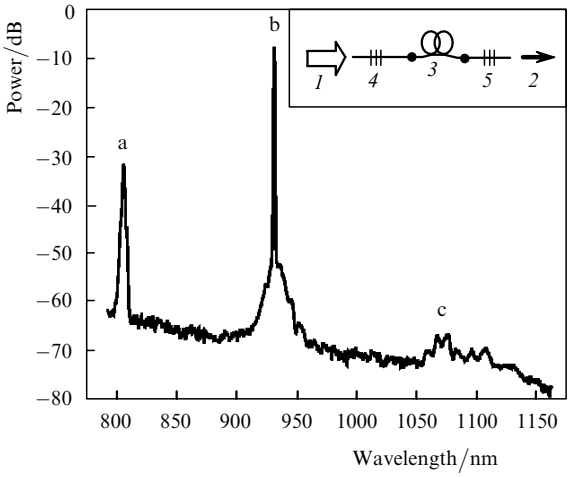

Figure 13. Emission spectrum of a Nd^{3+}-doped fibre laser at 925 nm: pump line (a), the 925-nm laser line (b), emission at 1060 nm (c). The inset shows the laser scheme: (*1*) pump radiation; (*2*) output radiation; (*3*) active fibre; (*4, 5*) FBGs.

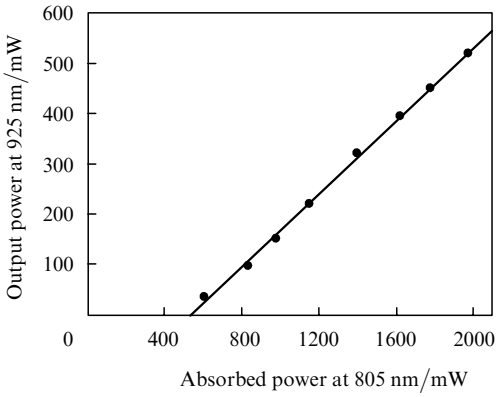

Figure 14. Dependence of the 925-nm output power of a Nd^{3+}-doped fibre laser on the absorbed pump power.

4.2 Yb^{3+}-doped fibre lasers

The energy level diagram of ytterbium ions in a silica glass is very simple, consisting of the $^2F_{7/2}$ ground level and the only excited $^2F_{5/2}$ level (Fig. 2). The absence of other energy levels up to the UV region means that both excited-state absorption and cooperative up-conversion should be absent in this system. This allows one to use ytterbium ions at much higher concentrations than concentrations of neodymium and erbium ions employed in corresponding fibre lasers. The use of fibres with high concentrations of active ions permits one, in turn, to reduce the length of the active fibre and, therefore, to decrease additional optical losses.

The absorption spectrum of such fibres, determined by electronic transitions between split energy levels, consists of the absorption band with two maxima at 915 and 976 nm. The luminescence spectrum consists of a narrow line at 980 nm and a band at 1035 nm, extending approximately up to 1200 nm (Fig. 15). The maximum absorption and luminescence cross sections virtually coincide and are 2.5×10^{-20} cm^2 [23] (silica glass was doped with aluminium and germanium). Note that pumping at 976 nm is more efficient due to a large absorption cross section. At the same time, pumping into the 915-nm band produces lasing at 976 nm. In addition, in this case the requirements to the stability of the pump wave with changing temperature are not strict due to a large width of the 915-nm band.

At present ytterbium lasers are the most popular clad-pumped fibre lasers, and they were described in numerous papers (see, for example, [59, 60]). In this review, we consider mainly the results obtained at the FORC, A.M. Prokhorov General Physics Institute, RAS.

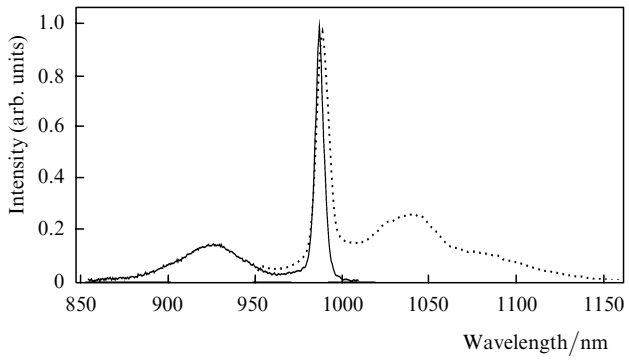

Figure 15. Absorption (solid curve) and luminescence (dotted curve) spectra of ytterbium ions in a silica glass.

The ytterbium-doped fibre laser uses a scheme with FBGs written both in the active fibre itself [61] and another fibre spliced then with the active fibre [62]. The parameters of active fibres used in these papers were as follows: the difference of the refractive indices of the core and cladding $\Delta n = (9 - 11) \times 10^{-3}$, the core diameter $2a = 4.5 - 5.5$ μm, and the concentration of ytterbium ions $(5 - 10) \times 10^{19}$ cm^{-3}. The size of the inner square cladding was 120×120 μm, which provided 100 % efficiency of fibre coupling with the fibre output of a pump semiconductor laser.

Figure 16a shows the typical dependence of the output power of an ytterbium-doped fibre laser at 1100 nm on the pump power. The slope efficiency of the laser is 80 %, corresponding to the quantum efficiency of about 90 %. Figure 16b shows the laser emission spectrum measured with a resolution of 0.01 nm; the width of the emission band is 0.1 nm.

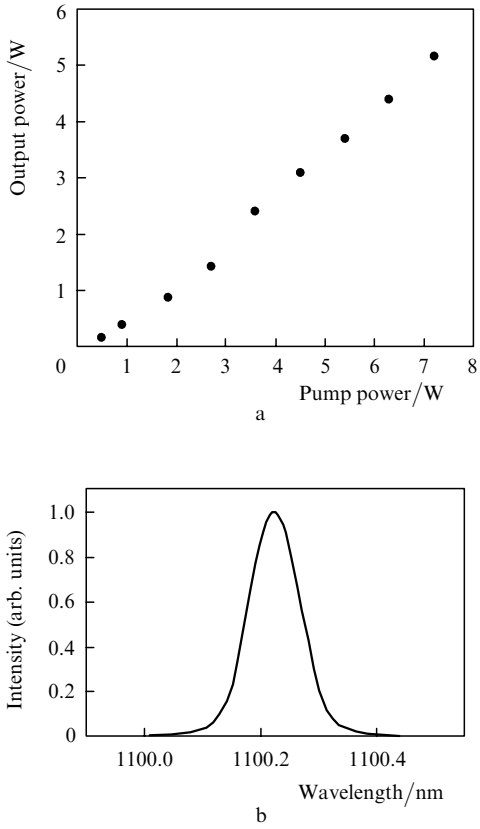

Figure 16. Dependence of the output power of a Yb^{3+}-doped fibre laser on the pump power (a) and the laser emission spectrum (b).

As mentioned above, a specific feature of clad-pumped fibre lasers is that it is difficult to produce complete inverse population in them because the effective pump cross section decreases proportionally to the ratio of areas of the fibre cladding and core. Therefore, the pump conversion efficiency strongly depends on the reabsorption of the signal by the part of non-inverted active ions. Absorption at the wavelengths 1000 and 1060 nm in the long-wavelength wing of the 976-nm absorption band of ytterbium ions is

approximately 2 % and 0.2 %, respectively, of absorption at 976 nm. At the same time, the luminescence band of ytterbium ions is located at 1035 nm and also has the extended long-wavelength tail. Therefore, the efficiency of the fibre laser is determined by the competition between luminescence and reabsorption, determining, in turn, the spectral dependence of the pump conversion efficiency.

Figure 17 shows the spectral dependence of the slope lasing efficiency for seven fibre lasers [63]. One can see that the maximum slope efficiency amounts to 80 % in the spectral region between 1.08 and 1.11 μm. It decreases down to 57 % at a wavelength of 1.049 μm due to reabsorption of radiation. The decrease in the lasing efficiency in the long-wavelength region is explained by a drastic decrease in the luminescence cross section.

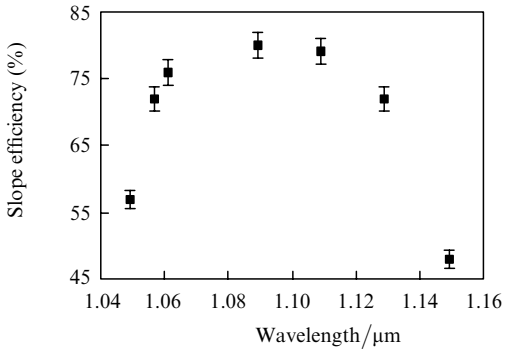

Figure 17. Spectral dependence of the slope efficiency of a Yb^{3+}-doped fibre laser pumped into a cladding.

Note that the above results are valid for the selected geometry of the active fibre, i.e., for the given ratio of areas of the core and cladding equal to ~ 500. The lasing efficiency in the short-wavelength region can be enhanced by increasing the core diameter. The use of fibres with claddings of a smaller size also seems promising. This is possible, taking into account the current trend for increasing the brightness of semiconductor lasers.

The use of active fibres with a diminished diameter of the inner cladding is especially important for the development of lasers emitting at 980 nm. Such lasers attract interest because they can be used for pumping high-power erbium-doped fibre amplifiers. One can see from Fig. 15 that absorption in this spectral region competes with luminescence, which requires the production of a high degree of population inversion to obtain lasing.

In [64], double-clad active fibres made of glasses of different compositions were used to obtain lasing at 980 nm. Figure 18 shows the refractive index profile of the preform of such a fibre fabricated by the MCVD method. The inner cladding of the fibre is made of a silica glass co-doped with GeO_2. The molar concentration of the impurity in the cladding was about 10 %, which provided the numerical aperture for pump radiation equal to 0.22. A supporting silica glass tube served as the outer cladding. The fibre core was doped with ytterbium and aluminium ions from solution. The inner-cladding and core diameters of the fibre were 25 and 10 μm, respectively. The concentration of Yb^{3+} ions was about 2×10^{19} cm^{-3}, which provided the absorption coefficient of 2.5 dB m^{-1} at 915 nm. The input FBG of the laser was written directly in the preliminary

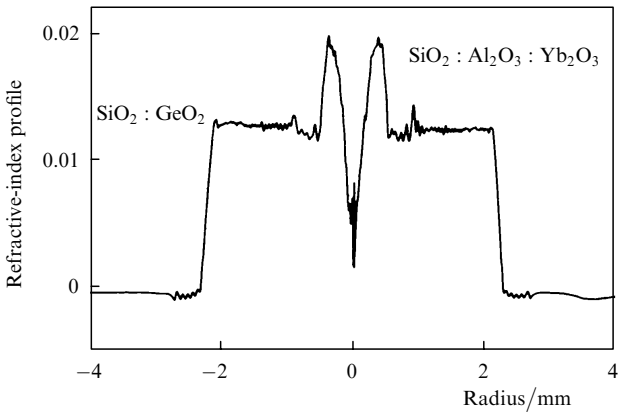

Figure 18. Refractive-index profile for an active-fibre preform with claddings made of glasses of different compositions.

hydrogen-loaded active fibre. The fibre laser was pumped by a semiconductor laser at 915 nm, by coupling ~ 5 W of pump power into the fibre of diameter 50 μm with the NA = 0.22.

The inset in Fig. 19 shows the emission spectrum of the 977.5-nm fibre laser. The maximum output power was obtained when an optical fibre of length 1.5 m was used. Figure 19 also shows the dependence of the output power on the pump power. The slope efficiency of the pump radiation conversion was 53 %, and the efficiency with respect to the absorbed pump power was 82 %.

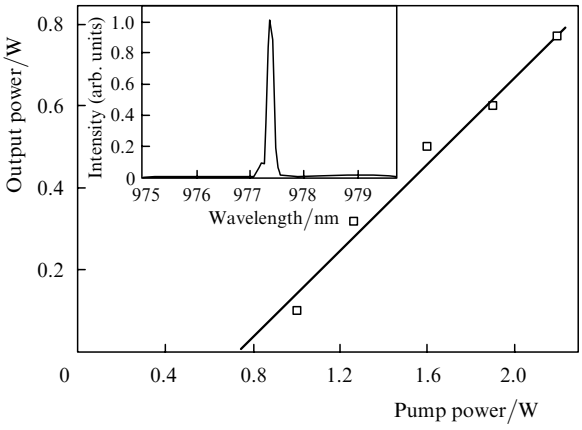

Figure 19. Dependence of the 977.5-nm output power of the laser on the pump power. The inset shows the laser emission spectrum.

To couple higher pump powers for obtaining higher output powers, a fibre with a microstructure cladding was used [65]. The numerical aperture of the inner cladding of diameter 20 μm was 0.7 and the output power at 980 nm was 1.4 W for the absorbed pump power of 2.5 W. A drawback of this laser design is the use of bulky mirrors in the resonator.

Optical fibres doped with Yb^{3+} ions were used in the first multimode laser with a resonator formed by multimode FBGs written in a multimode gradient fibre with the core diameter of 50 μm [66]. (Such FBGs were produced for the first time in Ref. [67].) An optical fibre with the core of diameter 16 μm doped with Yb^{3+} ions and the inner-

cladding diameter 50 μm was used as an active medium in the laser. Because of a small difference between the refractive indices of the activated core and inner cladding ($\Delta n = 0.003$), lasing at the fibre ends occurred not only in the fundamental mode but also in modes of the inner cladding, whose fields well overlapped with the core. Two multimode fibre lasers emitting at 1.03 and 0.98 μm were fabricated and studied. The output end of the active fibre was used as the output mirror in these lasers. The dependence of the output power of the 1036-nm laser on the pump power is shown in Fig. 20. The slope efficiency of the laser was 80 %, which corresponds to the 90 % slope quantum efficiency. The output power of the 978-nm laser was 1.5 W. These results demonstrate that multimode gratings can be efficiently used as mirrors in multimode lasers.

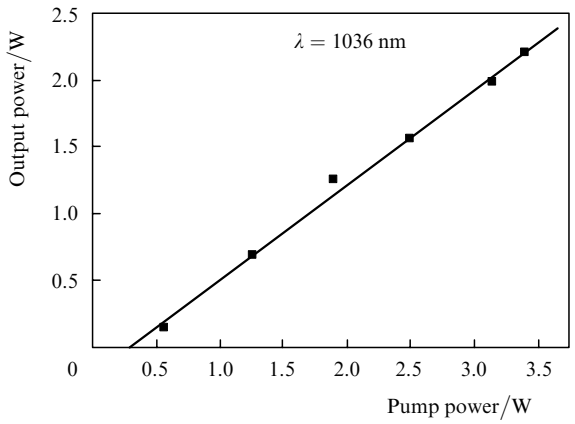

Figure 20. Dependence of the 1036-nm output power on the pump power for a multimode fibre laser.

Recently, special optical fibres, combining the active and passive fibres, find increasing applications in the development of high-power fibre lasers [42]. A laser using a triple fibre consisting of an active fibre and two passive fibres was demonstrated in Ref. [68] (Fig. 21). Four pump sources of a total power up to 100 W were used. The output cw power of the laser was 65 W at a wavelength of 1072 nm. The dependence of the output power of this laser on the pump power is shown in Fig. 22.

4.3 Er^{3+}-doped fibre lasers

The Er^{3+} ions in a silica glass have the luminescence band at 1.53 μm, which make it possible to fabricate fibre lasers and amplifiers operating in the spectral range from 1.53 to

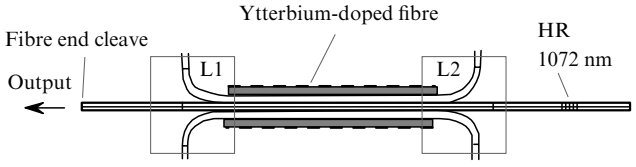

Figure 21. Simplified scheme of a triple-fibre laser. L1 and L2: branching points of the fibre; HR: highly reflecting FBG with the reflectivity close to 100% at 1072 nm. A fibre end cleave perpendicular to its axis was used as the output mirror.

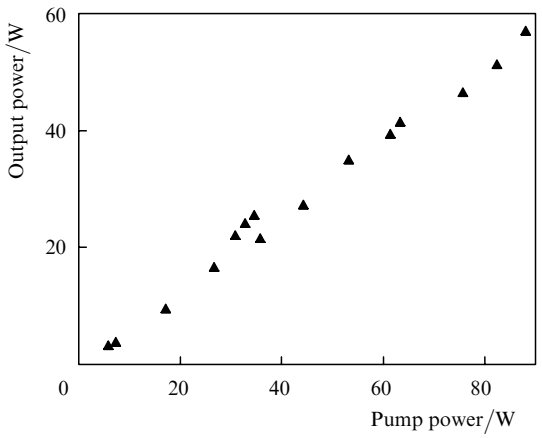

Figure 22. Dependence of the output power on the pump power for a Yb^{3+}-doped fibre laser pumped through passive fibres.

1.6 μm. The luminescence spectrum of Er^{3+} ions in an aluminogermanosilicate glass is shown in Fig. 23. Er^{3+}-doped fibre lasers operate according to the three-level scheme, which requires a high degree of population inversion.

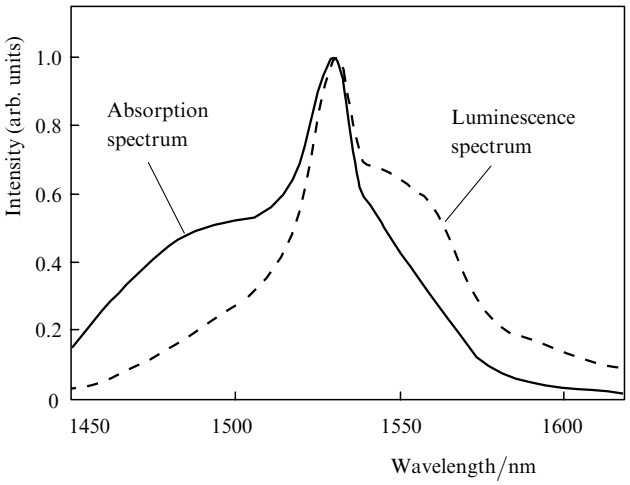

Figure 23. Absorption and luminescence spectra of erbium ions in an alumogermanosilicate glass.

The maximum of the absorption band virtually coincides with the luminescence maximum. Because of this, an optical fibre with a small diameter of the inner cladding allowing the achievement of high inversion degree was used in the first paper demonstrating a clad-pumped Er^{3+}-doped fibre laser [39]. The inner-cladding diameter was 22 μm and the numerical aperture was 0.18. The output power of 300 mW at 1540 nm was obtained upon 900-mW pumping at 980 nm. The slope efficiency was 40 %.

It is obvious that the output power in this case is restricted by the efficiency of pump power coupling into the inner cladding of a small diameter. At the same time, as one can see from Fig. 23, the luminescence band in the spectral region from 1.56 to 1.6 μm (the L band) dominates over absorption. This reduces the requirements on the degree of population inversion and allows one to use active

fibres with greater diameters of the inner cladding and, hence, to employ higher-power pump sources. This approach was realised in paper [69], where an active fibre with the inner-cladding diameter of 50 μm was used and the 1-W amplified signal in the L band was obtained. We can assume that such fibres can be also used for the development of lasers emitting in this spectral range.

To obtain lasing in the 1.53 – 1.6-μm range, optical fibres co-doped with Yb^{3+} and Er^{3+} ions are most often used. In such fibres, pump radiation at 976 nm is efficiently absorbed by Yb^{3+} ions, which transfer their excitation energy to Er^{3+} ions [70]. The energy transfer is possible because of the nearness of the $^2F_{5/2}$ level of ytterbium ions and the $^4I_{11/2}$ level of erbium ions.

One of the problems of manufacturing such a fibre is the appropriate selection and reproduction of the chemical composition of the fibre core. Thus, to reduce the probability of reverse energy transfer, it is necessary to decrease the lifetime of Er^{3+} ions at the excited $^4I_{11/2}$ level, which is achieved by using a phosphosilicate glass in the core. In addition, it is important to select properly the ratio of concentrations of the active ions. It was shown in Ref. [71] that the maximum lasing efficiency (~ 50 %) was achieved when the concentration of ytterbium ions exceeded that of erbium ions by a factor of 30.

At present, IPG produces commercial fibre lasers emitting more than 100 W in the spectral range from 1.53 to 1.62 μm. Note also that optical fibres doped with Er^{3+} and Yb^{3+} ions are used for the development of high-power single-frequency fibre lasers. Thus, a fibre laser emitting 5 W in the line of width less than 30 kHz (pumped by 25-W radiation) was demonstrated in Ref. [72].

4.4 Tm^{3+}-doped fibre lasers

As in the previous case, the efficient use of pumping into the cladding of fibres doped with Tm^{3+} ions is complicated because lasing in the 1.8 – 2-μm region occurs according to the three-level scheme. However, the situation is alleviated due to the presence of a strong absorption band centered at 787 nm caused by the $^3H_6 \rightarrow {}^3F_4$ transition. The absorption spectrum of a fibre doped with Tm^{3+} ions is shown in Fig. 24. In addition, the absorption and luminescence bands corresponding to the $^3H_4 \rightarrow {}^3H_6$ transition are well separated in a silica glass doped with Tm^{3+} ions, being located at 1600 and 1800 nm, respectively. The width of the luminescence band is ~ 300 nm [73]. This allows a sufficient degree of population inversion to be obtained, at which the signal reabsorption is negligible in the spectral region > 1.8 μm.

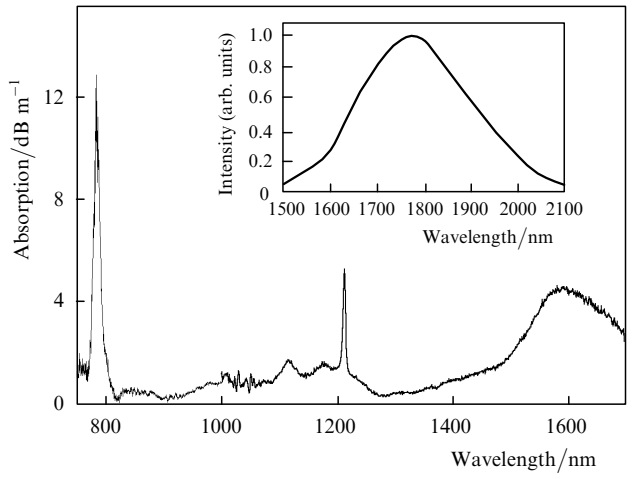

Figure 24. Absorption spectrum of a fibre doped with thulium ions. The inset shows the luminescence spectrum.

In the last years a number of papers devoted to the development of a clad-pumped Tm^{3+}-doped fibre laser were published. Such a laser pumped by 36.5 W at 787 nm and emitting 14 W at 2 μm with the slope efficiency of 46 % was demonstrated in Ref. [74]. A tunable Tm^{3+}-doped fibre laser was built in Ref. [75]. The tuning range of this laser was 230 nm (between 1860 and 2090 nm) and the maximum output power achieved 7 W at 1950 nm, decreasing down to 1 W at the tuning range boundaries.

4.5 Ho^{3+}-doped fibre lasers

The Ho^{3+} ions have the $^5I_7 \rightarrow {}^5I_8$ transition that can be used to obtain lasing at 2 μm. Figure 25 shows the luminescence spectrum of an optical fibre doped with Ho^{3+} ions excited by a krypton laser at 676 nm. This wavelength corresponds to the $^5I_8 \rightarrow {}^5I_4$ transition. The luminescence lifetime was 0.5 ms.

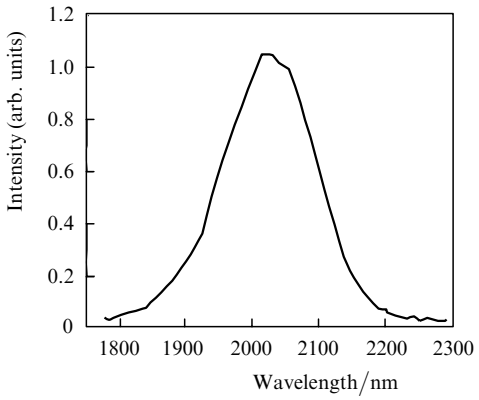

Figure 25. Luminescence spectrum of holmium ions in a silica glass.

In Ref. [17], a fibre laser was developed based on an aluminogermanosilicate fibre doped with Ho^{3+} ions by the impregnation method. The estimated concentration of Ho^{3+} ions was 1.2×10^{19} cm^{-3}. The difference of the refractive indices of the fibre core and cladding was ~ 0.08, and the cutoff wavelength for the first higher mode was 1.5 μm. Figure 26 shows the spectrum of optical losses of the fibre.

Because holmium-doped fibre lasers operate according to the three-level scheme, to achieve the required population inversion, the pump radiation should be efficiently absorbed. Because the most intense absorption bands are located in the visible region, the first holmium-doped fibre laser was pumped by an argon laser at 457.9 nm [76]. The fibre laser had a relatively low slope efficiency (1.7 %) and is maximum output power was 0.67 mW upon pumping by 85 mW.

It is obvious that the efficient practical application of holmium-doped fibre lasers requires pumping by semiconductor lasers. However, available high-power lasers emit at 750 nm and cannot be used for pumping into the absorption bands of holmium in the visible region. At the same time, pumping into the 900-nm absorption band cannot be efficient because of weak absorption in this band.

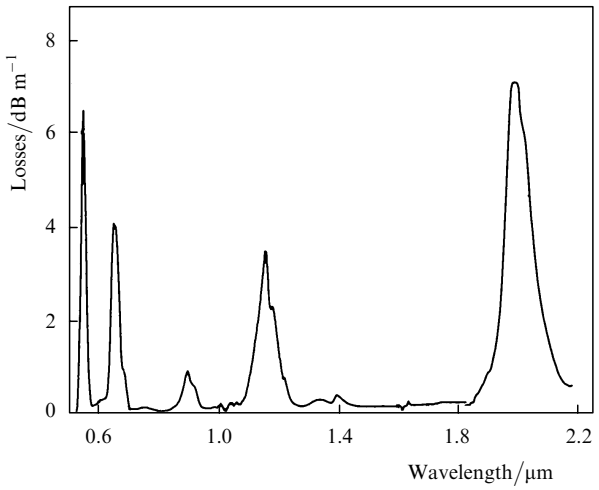

Figure 26. Absorption spectrum of a fibre doped with holmium ions.

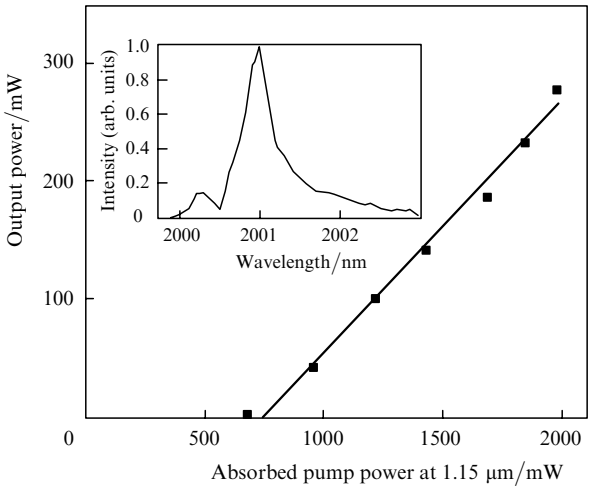

Figure 28. Dependence of the output power of a Ho^{3+}-doped fibre laser at 2 μm on the pump power. The inset shows the laser emission spectrum.

The efficient holmium-doped fibre laser was developed by using pumping by high-power ytterbium-doped fibre lasers pumped by diodes into cladding [17]. The holmium laser is pumped into the strong 1.15-μm absorption band corresponding to the $^5I_8 \rightarrow {}^5I_6$ transition [17]. The laser design is shown in Fig. 27. The laser uses a holmium-doped fibre with parameters presented above. A FBG had the resonance wavelength at 2001 nm with the linewidth 1 nm and the reflectivity above 99 %. The output end of the fibre was used as the output mirror with the reflectivity 4 %. The holmium laser was pumped into the core by a 1150-nm ytterbium-doped fibre laser with the maximum output power 3 W.

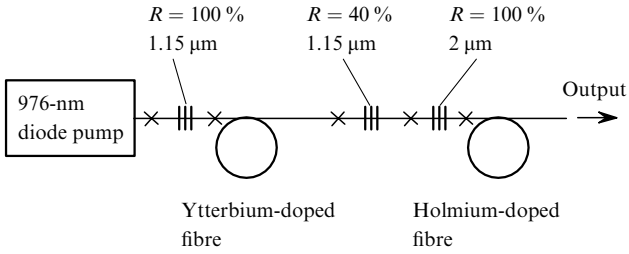

Figure 27. Scheme of a Ho^{3+}-doped fibre laser. Splicing points are indicated by crosses.

Figure 28 illustrates the dependence of the output power of the holmium laser on the absorbed pump power from the ytterbium laser for the resonator of length 4.5 m. The maximum output power 280 mW was achieved at the absorbed pump power equal to 2 W, and the slope efficiency was 20 %. The inset in Fig. 28 shows the emission spectrum of the holmium laser measured with the resolution of 0.2 nm. The lasing wavelength was determined by the resonance wavelength of the FBG, and the laser line width was ~ 0.4 nm [17].

The lasing efficiency of the holmium laser described above was considerably reduced due to high additional losses in the active fibre (0.65 dB m^{-1} at 1.3 μm). In principle, fibres with optical losses of the order of 0.01 dB m^{-1} can be fabricated, which will increase the slope lasing efficiency up to ~ 25 %. Note that the output power of modern semiconductor lasers with a fibre output with the fibre core diameter 100 μm achieves 20 W.

In recent years, holmium lasers co-doped with thulium [77] and ytterbium [78] ions were developed and studied. The lasers are pumped into the absorption bands of co-dopants, with the subsequent energy transfer to holmium ions. This allowed pumping into the cladding of the active fibre. The output power of the Tm : Ho-doped fibre laser was 5 W at 2.1 μm upon pumping by 20 W. The output power of the Yb : Ho-doped fibre laser was 0.85 W upon pumping by 11 W.

5. Raman fibre lasers

Fibre lasers based on fibres doped with rare-earth ions emit only in certain spectral ranges which do not cover the entire IR region. SRS in optical fibres can be used for the efficient wavelength conversion to obtain lasing virtually at any wavelength of the near-IR region. The design of a Raman laser and parameters of the fibre used for wavelength conversion depend on the pump wavelength and the specified wavelength of the converter. It is preferable to use an ytterbium-doped fibre laser for pumping due to its high efficiency in a broad spectral range.

The first efficient Raman lasers were developed in papers [59, 79–81]. In [82], an efficient Raman converter based on fibre multiplexers providing feedback was described. In this section, we consider different types of lasers developed and studied at FORC.

5.1 Single-stage Raman lasers

The simplest type of a Raman laser is a single-stage Raman laser. An optical fibre with the germanosilicate core ($\Delta\nu_{St} = 440-480$ cm^{-1}) converts radiation from an ytterbium-doped fibre laser to radiation in the spectral range between 1.1 and 1.22 μm.

In Ref. [54], the 1.09-μm radiation from an ytterbium laser was converted to the 1.15-μm radiation by using a standard Flexcore-1060 fibre in the Raman laser with optical losses equal to 0.8 dB km^{-1} at 1.06 μm. The Raman gain at 1.15 μm was 5.5 ± 0.5 dB km^{-1} W^{-1}. The length of the fibre was 500 m, and the reflectivity of the output FBG

was 20 %. Figure 29 shows the experimental dependence of the output power of the converter on the output power of the ytterbium laser for the fibre length of 500 m. Also, the theoretical dependence calculated using the model described in section 2.4 is presented. It follows from Fig. 29 that the conversion efficiency for radiation from the fibre laser exceeds 70 %.

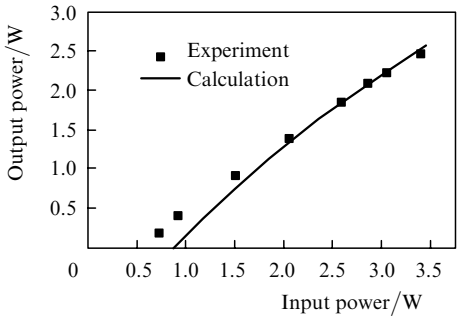

Figure 29. Dependence of the output power of a single-stage Raman germanosilicate fibre converter on the ytterbium laser power.

Optical fibres with the phosphosilicate glass core exhibit the additional Raman line at 1330 cm^{-1} (Fig. 10). As a rule, the molar content of phosphorous oxide in such fibres is 13 %–15 % and optical losses are ~ 1.8 dB km^{-1} at 1.06 μm and decrease approximately down to 1 dB km^{-1} at 1.5 μm. Single-stage Raman converters of radiation from an ytterbium-doped fibre laser based on these fibres give radiation in the region between 1.22 and 1.35 μm [83]. By using a neodymium-doped fibre laser for pumping, a Raman laser emitting at 1.24 μm with the conversion efficiency of ~ 70 % was developed [80].

Figure 30 shows the dependence of the output power of a Raman laser at 1234 nm on the power of a fibre laser emitting at 1060 nm. The emission spectrum of the Raman laser is shown in the inset in Fig. 30. A specific feature of the laser design is that the FBGs forming the resonator of the Raman laser were written directly in the phosphosilicate fibre. This reduced intracavity losses and enhanced the conversion efficiency.

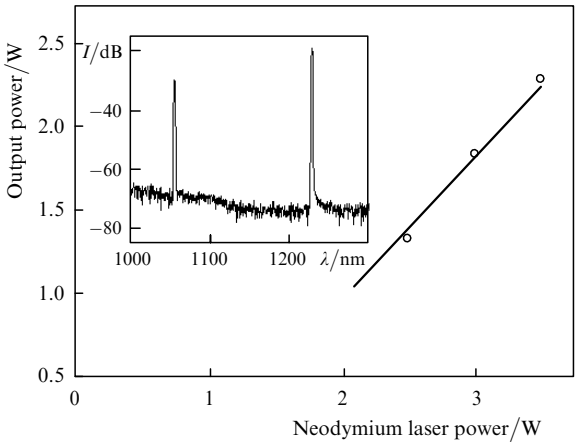

Figure 30. Dependence of the output power of a single-stage Raman laser on the pump power at the input to a phosphosilicate fibre. The inset shows the output emission spectrum of the Raman laser.

Of great interest is the development of Raman lasers based on optical fibres with a very high concentration (above 50 %) of GeO_2 in the fibre core. In this case, due to a higher nonlinearity of a germania glass compared to silica and a small diameter of the fibre core, the Raman gains amounting to a few hundreds dB km^{-1} W^{-1} can be obtained, which allows one to reduce considerably the active fibre length in the Raman laser. Thus, a Raman laser based on an optical fibre with the molar concentration of germanium dioxide in the core equal to 75 % and the Raman gain ~ 300 dB km^{-1} W^{-1} was demonstrated in Ref. [84]. The resonator length of the fibre laser was only 3 m. The efficiency of conversion of the 1.07-μm radiation from the ytterbium-doped fibre laser to radiation at 1.12 μm was 70 %. Figure 31 shows the corresponding dependence of the output power of the Raman laser on the pump power from the Yb-doped fibre laser.

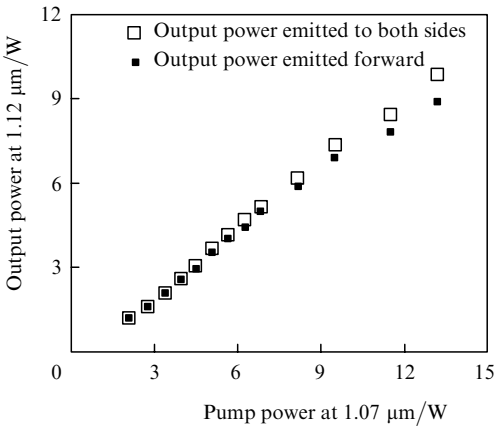

Figure 31. Dependence of the output power of a Raman germanate fibre laser on the pump power.

5.2 Multistage Raman lasers

To obtain lasing in the spectral region above 1.35 μm, it is necessary to use multistage Raman lasers. Thus, by using four-stage Raman conversion in a germanosilicate fibre, one can produce lasing in the spectral range between 1.35 and 1.45 μm upon pumping the fibre by radiation from an ytterbium-doped fibre laser. However, the increase in the number of stages considerably complicates the laser design due to the increase in the number of FBG pairs, which should have certain resonance wavelengths maintained with a high accuracy. In addition, FBGs introduce additional excess losses (~ 0.05 dB per grating), which reduces the conversion efficiency. Therefore, the search for new active media for Raman lasers is an urgent task.

A substantial step forward was achieved by using a fibre with the phosphosilicate core, in which amplification was obtained not only at the Stokes frequency of 1330 cm^{-1} but also at the frequency shifted by 440 cm^{-1} and corresponding to SRS in pure silica. Therefore, it became possible to use two different frequency shifts in the same optical fibre [85].

In Ref. [86], a Raman laser emitting at 1407 nm was developed, which used one conversion with the 1330-cm^{-1} shift and two conversions with the 440-cm^{-1} shift. The maximum output power at 1407 nm was 1 W and the conversion efficiency was 25 %. In Ref. [87], the same design

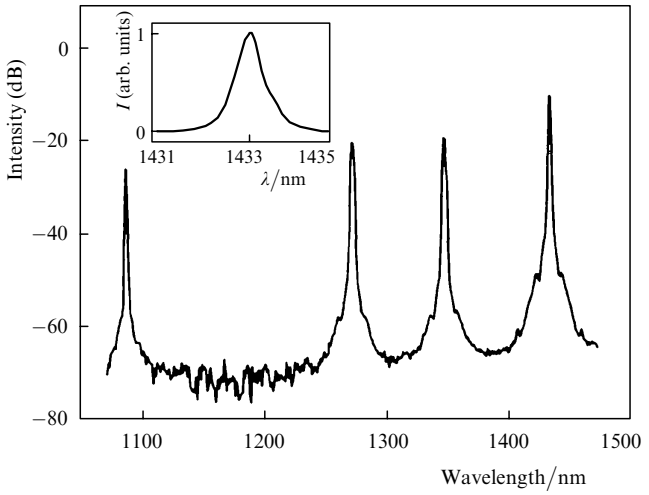

Figure 32. Emission spectrum of a Raman phosphosilicate fibre laser with the use of the 440-cm^{-1} and 1330-cm^{-1} Stokes shifts.

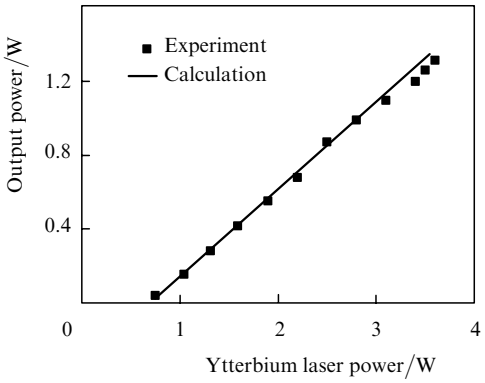

Figure 34. Dependence of the output power of a 1480-nm two-stage Raman phosphosilicate laser on the 1061-nm input power of an ytterbium laser.

was used in the laser emitting the maximum power of 1.3 W at 1430 nm (Fig. 32).

Of special interest are Raman lasers emitting in the 1.45 – 1.6-μm range corresponding to the spectral region used in optical communications. In particular, such lasers can be applied to pump Raman and erbium-doped fibre amplifiers. Lasing in this spectral range can be most conveniently obtained by using two-stage frequency conversion in phosphosilicate fibres. The dependence of the efficiency of such a laser on the pump power, the fibre length and the reflectivity of the output FBG was theoretically analysed in Ref. [53]. The calculations were performed using the parameters of a phosphosilicate fibre with the concentration of P_2O_5 equal to 13 %. The initial wavelength was 1061 nm and the final wavelength was 1480 nm. The optical losses of the phosphosilicate fibre were 1.55, 0.92, and 0.75 dB km^{-1} at the wavelengths 1061, 1240, and 1480 nm, respectively. The gains were 5.5 and 4 dB km^{-1} W^{-1} at the wavelengths 1240 and 1480 nm, respectively. In addition, the calculation took into account intracavity losses caused by splicing of the phosphosilicate fibre with a fibre in which FBGs were written and by additional scattering from FBGs. These additional losses were estimated as 8 %. Figure 33 shows the results of calculations. Figure 34 shows the experimental and calculated dependences of the output power of the Raman laser on the pump power from the ytterbium-doped fibre laser.

To increase the efficiency of the Raman converter, FBGs in Ref. [88] were written directly in a phosphosilicate fibre, which reduced intracavity losses, resulting in the 45 % conversion efficiency.

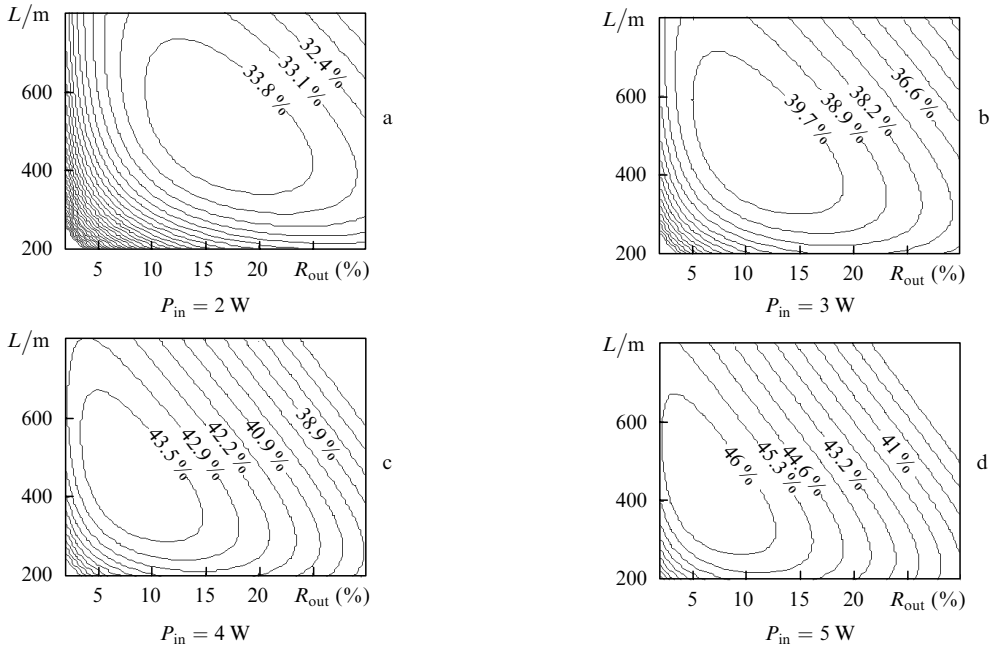

Figure 33. Dependences of the conversion efficiency (in %) of a two-stage Raman laser on the phosphosilicate fibre length L and the reflectivity R_{out} of the output grating for different input pump powers P_{in}.

5.3 Composite Raman lasers

The long-wavelength boundary of the efficient wavelength conversion in lasers described in section 5.2 is 1.6 μm. In the case of Raman lasers, it is determined by the two-stage Raman conversion in a phosphosilicate fibre and by the long-wavelength emission edge (1.12 μm) of ytterbium-doped fibre lasers, where the lasing efficiency exceeds 60 %. At the same time, the spectral range between 1.6 and 1.8 μm is also of interest for a number of applications.

Emission in this spectral region can be obtained by using a Raman laser based on a phosphosilicate optical fibre with two frequency shifts by 1330 cm^{-1} related to the P_2O_5 component and one frequency shift by 440 cm^{-1} related to a silica glass.

Unfortunately, phosphosilicate fibres have at present much higher optical losses than germanosilicate fibres (0.8 – 1 dB km^{-1} against 0.2 dB km^{-1} at 1.5 μm). As the wavelength further increases, optical losses in phosphosilicate fibres related to the edge of phonon absorption increase faster than losses in germanosilicate fibres. Therefore, the scheme, which uses simultaneously Stokes shifts caused by the phosphorous and silica components of the fibre, does not seem promising. At the same time, optical losses in germanosilicate fibres grow much slower, and in telecommunication optical fibres they are ~ 0.25 dB km^{-1} in this spectral region.

The use of germanosilicate optical fibres in Raman lasers requires the seven-stage frequency conversion to obtain radiation at wavelengths longer than 1.6 μm. Because such a laser design is complex and low-efficient due to a high total threshold pump power, it was proposed [89] to use a composite Raman laser, whose scheme is shown in Fig. 35. The laser consists of two parts: a two-stage phosphosilicate fibre converter and a single-stage germanosilicate fibre converter. The first and second parts of the converter produce radiation at 1533 and 1649 nm, respectively. The maximum output power at 1533 nm was 2.07 W upon pumping by a 8-W semiconductor laser. A standard telecommunication fibre with the zero chromatic dispersion wavelength shifted to 1.55 μm was used as an active medium at the second stage. Optical losses in this fibre were 0.2 and 0.25 dB km^{-1} at the wavelengths 1533 and 1649 nm, respectively. The small-signal gain at 1640 nm was 2.2 dB km^{-1} W^{-1}. The gain was measured with the help of a semiconductor laser emitting in this spectral range. Figure 36 shows the dependence of the output power of the 1649-nm Raman laser on the pump power.

Despite a low gain, the conversion efficiency for the 1533-nm radiation to the 1649-nm radiation was 63 %, the slope efficiency of conversion of the 1089-nm radiation from the ytterbium-doped fibre laser was 32 %, and the linewidth of the Raman laser was 0.35 nm (Fig. 36).

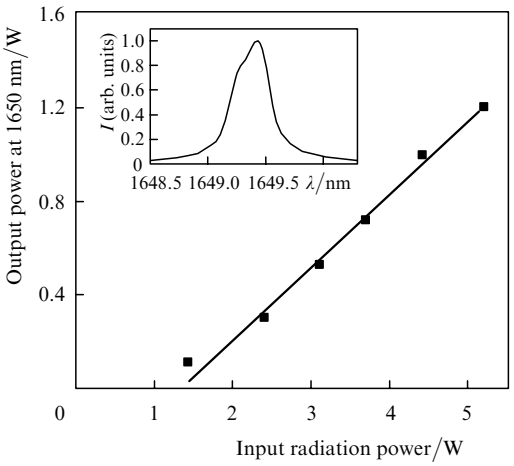

Figure 36. Dependence of the output power of a composite Raman laser on the ytterbium laser power at 1089 nm. The inset shows the emission spectrum of the composite laser.

Note that the use of the composite Raman laser provides emission in the spectral range between 1.6 and 1.75 μm. The expected output power is approximately the same because the required radiation wavelength of the ytterbium-doped fibre laser lies in this case in the 1.07 – 1.12-μm range, where the efficiency of this laser changes weakly.

To obtain laser radiation at 2 μm and at longer wavelengths, GeO_2 glass fibres should be used. The GeO_2 glass has a minimum of optical losses at 2 μm, where the Raman cross section exceeds that for a silica glass by an order of magnitude. In addition, the germania glass has a high photosensitivity, which allows FBG writing in a hydrogen-unloaded fibre [90].

In Ref. [91], a four-stage Raman germania glass fibre laser (Raman laser 1) emitting at 2.06 μm was developed. The laser was pumped by a two-stage Raman phosphosilicate fibre laser emitting at 1472 nm, which, in turn, was pumped by a 1057-nm ytterbium-doped fibre laser. Figure 37 shows the scheme of this Raman laser, and its emission spectrum is presented in Fig. 38.

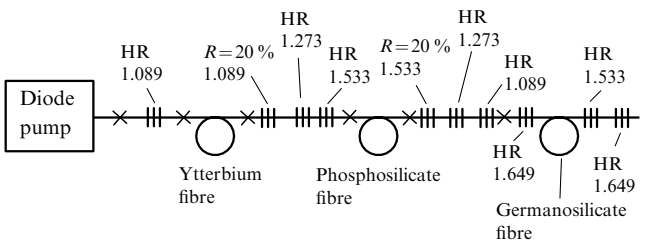

Figure 35. Scheme of a composite Raman laser. The crosses indicate splicing points; the resonance wavelengths are indicated (in μm) near each of the gratings.

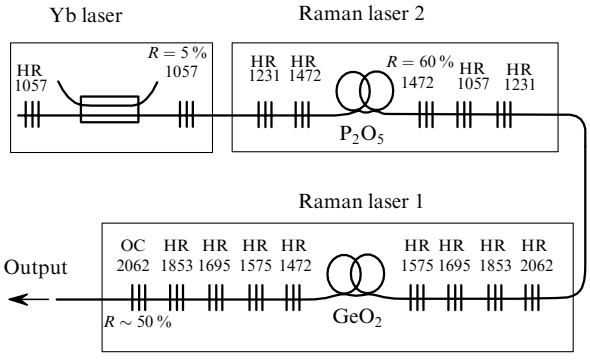

Figure 37. Scheme of a 2.06-μm four-stage Raman fibre laser. OC: output coupler. The resonance wavelengths are indicated (in nm) near each of the gratings.

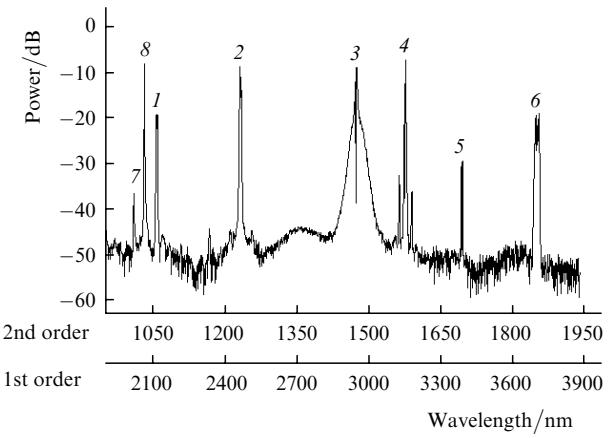

Figure 38. Output emission spectrum of a four-stage Raman laser: (*1*) 1057-nm pump radiation from an ytterbium laser; (*2*, *3*) emission from two stages of Raman phosphosilicate fibre laser 2 (at 1231 and 1472 nm); (*4*, *5*, *6*) emission from the first three stages of four-stage Raman laser 1 (at 1575, 1695, and 1853 nm); (*7*) emission at the maximum of the Raman gain at 2017 nm corresponding to the 440-cm^{-1} frequency shift from 1853 nm; (*8*) 2062-nm emission from the fourth stage of Raman laser 1.

6. Conclusions

We showed in the review that optical fibres doped with various rare-earth ions have been used for the development of fibre lasers emitting in various spectral regions. Thus, Nd^{3+}-doped fibre lasers emit at 0.92 and 1.06 μm; Yb^{3+}-doped fibre lasers emit in the region 0.98–1.15 μm; Er^{3+}- and Er^{3+} : Yb^{3+}-doped fibre lasers emit in the region 1.53–1.6 μm; and Tm^{3+}- and Ho^{3+}-doped fibre lasers emit in the regions 1.5–2 μm and 2–2.1 μm, respectively. To obtain moderate lasing powers, it is necessary to use pumping into the fibre cladding. In this case, the fibre structure for the pump radiation can be made of a silica glass and a polymer, silica glasses of different compositions, and also a microstructure cladding can be used.

The use of photoinduced FBGs as mirrors substantially simplified the design of lasers. Note here that multimode gratings also can be used.

Raman lasers based on optical fibres of different compositions and FBGs are used for conversion of radiation from fibre lasers to radiation at any wavelength in the spectral region between 1.15 and 1.65 μm. The conversion efficiency is 30 %–70 % depending on the number of conversion stages. The use of a germania glass fibre expands this region up to 2 μm.

Therefore, fibre lasers considered in the review produce moderate-power radiation at any wavelength in the spectral range between 0.9 and 2 μm, covering virtually the entire near IR-region.

Acknowledgements. The authors thank I.A. Bufetov for placing the experimental results at our disposal.

References

1. Snitzer E. *Phys. Rev. Lett.*, **7**, 444 (1961).
2. Mears R.J., Reekie L., Jancie I.M., Payne D.N. *Proc. Opt. Fiber Commun. Conf. OFC'87* (Reno, USA, 1987) Vol. 3, p. 167.
3. Hill K.O., Fujii Y., Johnson D.C., Kawasaki B.S. *Appl. Phys. Lett.*, **32**, 647 (1978).
4. Meltz G., Morey W.W., Glenn W.H. *Opt. Lett.*, **14**, 823 (1989).
5. Zyskind J.L., Mizrahi V., DiGiovanny D.J., Sulhoff J.W. *Electron. Lett.*, **28**, 1385 (1992).
6. Dong L., Loh W.H., Caplen J.E., Hsu K., Minelli J.D., Reekie L. *Opt. Lett.*, **22**, 694 (1997).
7. Dianov E.M., Prokhorov A.M. *IEEE J. Sel. Topics Quantum Electron.*, **6**, 1022 (2000).
8. Dominic V., MacCormack S., Waarts R., Sanders S., Bicknese S., Dohle R., Wolak E., Yeh P.S., Zucker E. *Electron. Lett.*, **35**, 1158 (1999).
9. Platonov N.S., Gapontsev D.V., Gapontsev V.P., Shumilin V. *Proc. CLEO'2002* (Long Beach, USA, 2002) p. CPDC3.
10. Reichel V., Unger S., Brückner S., Mörl K., Müller H.-R., Kirchhof J., Sandrock T., Harchack A. *Photon. West Conf.* (San Jose, USA, 2003) p. 4974-23.
11. Zellmer H., Liem A., Limpert J., Schreiber T., Höfer S., Tünnermann A. *XII Int. Laser Phys. Workshop* (Hamburg, Germany, 2003) p. 4.4.1.
12. Ueda K.-I., Sekiguchi H., Kan H. *Proc. CLEO'2002* (Long Beach, USA, 2002) p. CPDC4.
13. Gapontsev V.P. *XII Int. Laser Phys. Workshop* (Hamburg, Germany, 2003) p. PS3.
14. Mears R.J., Reekie L., Poole S.B., Payne D.N. *Electron. Lett.*, **21**, 738 (1985).
15. Bufetov I.A., Dudi V.V., Shubin A.V., Senatorov A.K., Dianov E.M., Grudinin A.B., Goncharov S.E., Zalevskii I.D., Gur'yanov A.N., Yashkov M.V., Umnikov A.A., Vechkanov N.N. *Kvantovaya Elektron.*, **33**, 1035 (2003) [*Quantum Electron.*, **33**, 1035 (2003)].
16. Gandy H.W., Ginther R.J. *Proc. IRE*, **50**, 2113 (1962).
17. Kurkov A.S., Dianov E.M., Medvedkov O.I., Ivanov G.A., Aksenov V.A., Paramonov V.M., Vasiliev S.A., Pershina E.V. *Electron. Lett.*, **36**, 1015 (2000).
18. Bjarklev A. *Optical Fiber Amplifiers: Design System Applications* (Boston, London: Artech House, 1993).
19. Becker P.C., Olsson N.A., Simpson J.R. *Erbium-Doped Fiber Amplifiers Fundamentals Technology* (San Diego: Acad. Press, 1999).
20. Gandy H.W., Ginther R.J., Weller J.R. *J. Appl. Phys.*, **38**, 3030 (1967).
21. Hanna D.C., Jauncey I.M., Percival R.M., Perry I.R., Smart R.G., Suni P.J., Townsend J.E., Tropper A.C. *Electron. Lett.*, **24**, 1222 (1988).
22. Gapontsev V.P., Samartsev I.E., Zayats A.A., Loryan R.R. *Proc. Conf. Adv. Solid State Lasers* (Hilton Head, USA, 1991, WC1-1) p. 214.
23. Pask H.M., Carman R.J., Hanna D.C., Tropper A.C., Mackechnie C.J., Barber P.R., Dawes J.M. *IEEE J. Sel. Topics Quantum Electron.*, **1**, 1 (1995).
24. Kashyap R. *Fiber Bragg Gratings* (San Diego: Acad. Press, 1999).
25. Tamir T. (Ed.) *Topics Appl. Phys., Vol. 7. Integrated Optics* (Berlin, Heidelberg: Springer-Verlag, 1975).
26. Othonos A. *Rev. Sci. Instrum.*, **68**, 4309 (1997).
27. Hill K.O., Malo B., Bilodeau F., Johnson D.C., Albert J. *Appl. Phys. Lett.*, **62**, 1035 (1993).
28. Poole S.B., Payne D.N., Mears R.J., Fermann M.E., Laming R.I. *IEEE J. Lightwave Techn.*, **4**, 870 (1986).
29. Dianov E.M., Karpov V.I., Kurkov A.S., Protopopov V.N., Devyatykh G.G., Guryanov A.N., Gusovskiy D.D., Kobis S.V., Zverev Yu.B. *Proc. XXI Europ. Conf. Opt. Commun.* (Brussels, 1995) Vol. 2, p. 721.
30. Bosko P.L. *Proc. Opt. Fiber Commun. Conf. OFC'89* (Houston, 1989) Vol. 5, p. 20.
31. Abramov A.A., Bubnov M.M., Dianov E.M., Voronkov A.E., Guryanov A.N., Devjatykh G.G., Ignatjev S.V., Zverev V.B., Karpychev N.S., Mazavin S.M. *Proc. CLEO'90* (Anaheim, USA, 1990) Vol. 7, p. 404.
32. Wada A., Tanaka D., Sakai T., Nozava T., Aikawa K., Tamauchi R., in *Opt. Amplifiers Their Applications, OSA Techn. Dig. Ser.*, **17**, 222 (1992).

33. Dianov E.M., Golant K.M., Khrapko R.R., Kurkov A.S., Protopopov V.N., Semenov S.L. *Opt. Mater.*, **3**, 181 (1994).
34. Kurkov A.S., Laptev A.Yu., Dianov E.M., Guryanov A.N., Karpov V.I., Paramonov V.M., Medvedkov O.I., Umnikov A.A., Protopopov V.N., Vechkanov N.N., Vasiliev S.A., Pershina E.V. *Proc. SPIE Int. Soc. Opt. Eng.*, **4083**, 118 (2000).
35. Ainslie B.J. *J. Lightwave Techn.*, **9**, 220 (1991).
36. Snitzer E., Po H., Hakimi F., Tumminelli R., McCollum B.C. *Proc. Conf. Opt. Fiber Sensors* (New Orleans, 1988) PD5.
37. Zenteno L. *IEEE J. Lightwave Techn.*, **11**, 1435 (1993).
38. Liu A., Ueda K. *Opt. Commun.*, **132**, 511 (1996).
39. Minelly J.D., Chen Z.J., Laming R.L., Caplen J.E. *Proc. XXI Europ. Conf. Opt. Commun.*, **2**, 917 (1995).
40. Sahu J.K., Renaud C.C., Furusawa K., Selvas R., Alvarez-Chavez J.A., Richardson D.J., Nilsson J. *Electron. Lett.*, **37**, 1118 (2001).
41. Goldberg L., Koplov J.P., Kliner D. *Opt. Lett.*, **24**, 673 (1999).
42. Grudinin A.B., Payne D., Turner P.W., Zervas M.N., Ibsen M., Durkin M.K. Int. patent WO 00/67350 (Priority data 30.04.99).
43. Stolen R.H., Ippen E.P., Tynes A.R. *Appl. Phys. Lett.*, **20**, 62 (1972).
44. Aksenov V.A., Bazarov E.N., Belov A.V., Dianov E.M., Ivanov G.A., Isaev V.A., Koltashev V.V., Makovetskii A.A., Nametov K.M., Plotnichenko V.G., Chamorovskii Yu.K. *Neorg. Mater.*, **34**, 1218 (1998).
45. Dianov E.M., Fursa D.G., Abramov A.A., Belovolov M.I., Bubnov M.M., Shipulin A.V., Prokhorov A.M., Devyatykh G.G., Gur'yanov A.N., Khopin V.F. *Kvantovaya Elektron.*, **21**, 807 (1994) [*Quantum Electron.*, **24**, 749 (1994)].
46. Grubb S.G., Erdogan T., Mizrahi Y., Strasser T., Cheung W.Y., Reed W.A., Lemaire P.J., Miller A.E., Kosinski S.G., Nykolyak G., Becker P.C., Pechkam D.W. *Proc. Opt. Amplifiers Their Applications* (Brekenridge, 1994) p. PD-3.
47. Dianov E.M., Prokhorov A.M. Patent of the Russian Federation No. 2095902 (10.11.97); US Patent 5 833 700 (Priority data 17.11.98).
48. Bubnov M.M., Dianov E.M., Egorova O.N., Semjonov S.L., Guryanov A.N., Khopin V.F., DeLiso E.M. *Proc. SPIE Int. Soc. Opt. Eng.*, **4083**, 12 (2000).
49. Reed W.A., Coughran W.C., Grubb S.G. *Proc. Opt. Fiber Commun. Conf. OFC'95* (San Diego, USA, 1995) p. 107.
50. Vareille G., Audouin O., Desurvire E. *Electron. Lett.*, **34**, 675 (1998).
51. Rini M., Cristiani I., Degiorgio V. *IEEE J. Quantum Electron.*, **36**, 1117 (2000).
52. Bufetov I.A., Dianov E.M. *Kvantovaya Elektron.*, **30**, 873 (2000) [*Quantum Electron.*, **30**, 873 (2000)].
53. Kurukitkoson N., Suguhara H., Turitsyn S.K., Egorova O.N., Kurkov A.S., Paramonov V.M., Dianov E.M. *Electron. Lett.*, **37**, 1281 (2001).
54. Rini M., Cristiani I., Degiorgio V., Kurkov A.S., Paramonov V.M. *Opt. Commun.*, **203** (1-2), 139 (2002).
55. Po H., Snitzer E., Tuminelli R., Zenteno L., Hakimi F., Cho N.M., Haw T. *Proc. Opt. Fiber Commun. Conf. OFC'89* (Houston, USA, 1989) PD7.
56. Zellmer H., Tünnermann A., Welling H., Reichel V. *Proc. Conf. Opt. Amplifiers Their Applications, OSA Trends Opt. Photon. Ser.*, **16**, 137 (1997).
57. Dianov E.M., Belov A.V., Bufetov I.A., Protopopov V.N., Gur'yanov A.N., Gusovskii D.D., Kobis' S.V. *Kvantovaya Elektron.*, **24**, 3 (1997) [*Quantum Electron.*, **27**, 1 (1997)].
58. Jackson S.D., Li Y. *IEEE J. Quantum Electron.*, **39**, 1118 (2003).
59. Inniss D., DiGiovanni D.J., Strasser T.A., Hale A., Headley C., Stentz A.J., Pedrazzani R., Tipton D., Kosinski S.G., Brownlow D.L., Quoi K.W., Kranz K.S., Huff R.G., Espindola R., Le Grange J.D., Jakobovich-Veselka G., Boggavarapu B., He X., Caffey D., Gupta S., Srinivasan S., McEuen K., Patel R. *Proc. CLEO'97* (Baltimore, USA, 1997) CPD31.
60. Muendel M., Engstrom B., Kea D., Laliberte B., Minns R., Robinson R., Rockney B., Zhang Y., Collins R., Gavrilovic P., Rowley A. *Proc. CLEO'97* (Baltimore, USA, 1997) CPD30.
61. Kurkov A.S., Medvedkov O.I., Karpov V.I., Vasiliev S.A., Lexin O.A., Dianov E.M., Gur'yanov A.N., Laptev A.A., Umnikov A.A., Vechkanov N.I. *Proc. Opt. Fiber Commun. Conf. OFC'99* (San Diego, USA, 1999, WM4) p. 205.
62. Kurkov A.S., Karpov V.I., Laptev A.Yu., Medvedkov O.I., Dianov E.M., Gur'yanov A.M., Vasil'ev S.A., Paramonov V.M., Protopopov V.N., Umnikov A.A., Vechkanov N.I., Artyushenko V.G., Fram Yu. *Kvantovaya Elektron.*, **27**, 239 (1999) [*Quantum Electron.*, **29**, 516 (1999)].
63. Kurkov A.S., Paramonov V.M., Medvedkov O.I., Vasiliev S.A., Dianov E.M. *Proc. Conf. Opt. Amplifiers Their Application* (Quebec City, Canada, 2000).
64. Kurkov A.S., Dianov E.M., Paramonov V.M., Medvedkov O.I., Vasiliev S.A., Solodovnikov V.V., Zhilin V., Laptev A.Yu., Umnikov A.A., Guryanov A.N. *Conf. Dig. CLEO-2001* (Baltimore, USA, 2001) p. 216.
65. Selvas R., Yla-Jarkko K., Alam S.U., Nilsson J., Turner P.W., Moore J., Sahu J.K., Grudinin A.B. *Proc. Opt. Fiber Commun. Conf. OFC'2003* (Atlanta, USA, 2003) p. TuL4.
66. Kurkov A.S., Medvedkov O.I., Vasiliev S.A., Paramonov V.M., Grukh D.A., Dianov E.M., Guryanov A.N., Umnikov A.A. *Techn. Dig. IQEC/LAT-2002* (Moscow, 2002) p. LSuD4.
67. Mizunami T., Gupta S., Yamao T., Shimomura T. *Proc. Conf. IOOC-ECOC'97* (Edinburg, 1997) Vol. 3, p. 182.
68. Bufetov I.A., Melkoumov M.A., Bubnov M.M., Kravtsov K.S., Semjonov S.L., Shubin A.V., Dianov E.M. *XIII Int. Laser Phys. Workshop* (Trieste, 2004) p. 214.
69. Bousselet P., Bettiati M., Gasca L., Lambelet P., Leplingard F., Bayart D. *Proc. Opt. Amplifiers Their Applications Conf.* (Stresa, Italy, 2001, OWC-3).
70. Townsend J.E., Barnes W.L., Jedzejewski K.P., Grubb S.G. *Electron. Lett.*, **27**, 1858 (1991).
71. Vienne G.G., Caplen J.E., Dong L., Minelly J.D., Nilsson J., Payne D.N. *J. Lightwave Techn.*, **16**, 1990 (1998).
72. Alam S., Yla-Jarkko K.H., Chryssou C.E., Grudinin A.B. *Proc. XXIX Europ. Conf. Opt. Commun. ECOC'03* (Rimini, Italy, 2003) Vol. 3, We2.6.
73. Hanna D.C., Percival R.M., Smart R.G., Tropper A.C. *Opt. Commun.*, **75**, 283 (1989).
74. Hayward A., Clarkson W.A., Turner P.W., Nilsson J., Grudinin A.B. Hanna D.C. *Electron. Lett.*, **36**, 711 (2000).
75. Clarkson A., Barnes N.P., Turner P.W., Nilsson J., Hanna D.C. *Opt. Lett.*, **27**, 1989 (2002).
76. Hanna D.C., Percival R.M., Smart R.G. *Electron. Lett.*, **25**, 593 (1989).
77. Jackson S.D., Mossman S. *Appl. Phys. B*, **77**, 489 (2003).
78. Jackson S.D., Mossman S. *Appl. Opt.*, **42**, 3546 (2003).
79. Grubb S.G., Strasser T., Cheung W.Y., Reed W.A., Mizrahi Y., Erdogan T., Lemaire P.J., Vengsarkar A.M., Di Djovanni D.J., Pechkam D.W., Rockney B.H. *Proc. Top. Meet. Opt. Amplifiers Their Applications* (Davos, 1995) p. 197.
80. Dianov E.M., Bufetov I.A., Bubnov M.M., Grekov M.V., Shubin A.V., Vasil'ev S.A., Medvedkov O.I., Semenov S.L., Egorova O.N., Gur'yanov A.N., Khopin V.F., Yashkov M.V., Varelas D., Iokko A., Konstantini D., Lumberger H.G., Salate R.P. *Kvantovaya Elektron.*, **29**, 97 (1999). [*Quantum Electron.*, **29**, 935 (1999)].
81. Karpov V.I., Dianov E.M., Paramonov V.M., Medvedkov O.I., Bubnov M.M., Semyonov S.L., Vasiliev S.A., Protopopov V.N., Egorova O.N. *Opt. Lett.*, **24**, 887 (1999).
82. Chernikov S.V., Taylor J.R., Platonov N.S., Gapontsev V.P., Kuppers F., Mattheus A., Gabitov I. *Proc. OFC'97* (Dallas, USA, 1997) p. 345.
83. Kurkov A.S., Dianov E.M., Paramonov V.M., Gur'yanov A.N., Laptev A.Yu., Khopin V.F., Umnikov A.A., Vechkanov N.N., Medvedkov O.I., Vasil'ev S.A., Bubnov M.M., Egorova O.N., Semenov S.L., Pershina E.V. *Kvantiovaya Elektron.*, **30**, 791 (2000) [*Quantum Electron.*, **30**, 791 (2000)].
84. Bufetov I.A., Mashinsky V.M., Neustruev V.B., Shubin A.V., Medvedkov O.I., Dianov E.M., Guryanov A.M., Khopin V.F., Salgansky M.Yu. *Proc. CLEO'2004* (San Francisco, 2004) p. CMD1.

85. Bufetov I.A., Dianov E.M., Kurkov A.S. Patent of the Russian Federation, No. 2158458 (08.02.2000).
86. Dianov E.M., Bufetov I.A., Bubnov M.M., Vasiliev S.A., Medvedkov O.I. *Opt. Lett.*, **25**, 402 (2000).
87. Kurkov A.S., Dianov E.M., Paramonov V.M., Medvedkov O.I., Vasiliev S.A., Pershina E.V., Guryanov A.N., Laptev A.A., Umnikov A.A., Vechkanov N.N. *Proc. SPIE Int. Soc. Opt. Eng.*, **4083**, 126 (2000).
88. Bufetov I.A., Bubnov M.M., Larionov Y.V., Melkoumov M.A., Rybaltovsky A.A., Semjonov S.L., Dianov E.M., Vartapetov S.K., Obidin A.Z., Kurzanov M.A. *Proc. CLEO'2002* (Long Beach, USA, 2002) p. 480.
89. Dianov E.M., Kurkov A.S., Medvedkov O.I., Paramonov V.M., Egorova O.N., Kurukitkoson N., Turitsyn S.K. *Laser Phys.*, **13**, 397 (2003).
90. Mashinsky V.M., Medvedkov O.I., Neustruev V.B., Dvoyrin V.B., Vasiliev S.A., Dianov E.M., Khopin V.F., Guryanov A.N. *Proc. XXIX Europ. Conf. Opt. Commun.* (Rimini, Italy, 2003) Vol. 2, p. 210.
91. Dianov E.M. *XXX Europ. Conf. Opt. Commun. ECOC'04* (Stokholm, 2004) p. We1.3.1.